

***AB INITIO STUDY OF ELECTRONIC, MECHANICAL AND OPTICAL
PROPERTIES OF CH₃NH₃PbI₃ FOR PHOTOVOLTAIC APPLICATION***

TRUPHENA JEPKORIR KIPKWARKWAR

**A Research Thesis Submitted to the Institute of Post Graduate Studies of Kabarak
University in Partial Fulfillment of the Requirement for the Award of Master of
Science in Physics**

KABARAK UNIVERSITY

NOVEMBER,2021

DECLARATION

1. I do by declare that:

- i. This thesis is my original work prepared with no other than the indicated sources and to the best of my knowledge it has not been presented for the award of a degree in any university or college.
- ii. The work has not in-cooperated material from other works or a paraphrase of such material without due and appropriate acknowledgement
- iii. The work has been subjected to processes of anti-plagiarism and has met Kabarak University 15 per cent similarity index threshold

2. I do understand that issues of academic integrity are paramount and therefore I may be suspended or expelled from the University or my degree may be recalled for academic dishonesty or any other related academic malpractices.

Signed: _____

Name: Truphena J. Kipkwarkwar

Date: _____

Adm. No. GMS/M/0936/08/16

RECOMMENDATION

To the Institute of Postgraduate Studies:

The research thesis entitled “*Ab initio* Study of Electronic, Mechanical and Optical Properties of $\text{CH}_3\text{NH}_3\text{PbI}_3$ for Photovoltaic Application” and written by **Truphena J. Kipkwarwar** is presented to the Institute of Postgraduate Studies of Kabarak University. We have reviewed the research thesis and recommend it to be accepted in partial fulfilment of the requirement for award of Master of Science in Physics.

Signature:.....

Date:.....

Dr. Phillip O. Nyawere

Department of Biological and Physical Sciences

Kabarak University

Signature:.....

Date:.....

Dr. Christopher Maghanga

Department of Biological and Physical Sciences

Kabarak University

COPYRIGHT

©2021

Truphena J. Kipkwarwar

All rights reserved. No part of this Thesis may be reproduced or transmitted in any form by means of either mechanical, including photocopying, recording or any other information storage or retrieval system without permission in writing from the author or Kabarak University.

DEDICATION

This work is dedicated to my parents, husband Daniel B. Mengich and children, Jayden and Imani.

ACKNOWLEDGEMENT

I first and foremost acknowledge God for His providence during the period of this study. I would like to appreciate deeply Dr. Phillip O. Nyawere for the constant encouragement and discussions concerning my work, introducing me to Computational Physics and inviting me with the Kabarak University Physics team to various workshops organized by research group CTheP which gave me a platform to network with other DFT experts and broaden my scope on DFT. This work wouldn't have been successful without the input of Dr. Christopher Maghanga for constant encouragement and support during my course work and constructive discussions and criticisms of my work. Great appreciation to the School of Science Engineering and Technology (SSET) and the entire Physics Department for all the support they granted me during my Masters course. I would like to thank the Members of Kabarak University ICT Department lead by Reuben Sirma for their support in installing Ubuntu, Quantum Espresso and other programs used in this work.

Special regards to the Institute of Post Graduate School (IPGS) for all the support they gave me during the defense of my proposal and thesis. My deep gratitude goes to James .S. Sifuna, for broadening my scope on DFT and his continuous encouragement to grow in DFT. Thanks also to Dr. Elicah N. Wabululu for introducing me to hands on the Quantum Espresso code and constant encouragement during the entire period of my research. The Center for High-Performance Computing (CHPC), Cape Town, South Africa is thanked for the provision of HPC facility used in all the computation in this thesis. Finally special thanks to my husband Daniel B. Mengich, children Jayden Baruett and Imani Daniella, parents Shadrack Kimugo and Mary Ng'otie and Sisters Daisy and Lydia for their prayers and continuous support to me throughout this journey.

ABSTRACT

The ever increasing need of energy in third world countries has necessitated the need for coming up with measures of seeking alternative energy sources. Solar energy is one of the most important alternative sources of energy because of its abundance in these regions. Up to this time, the use of the first and second generations solar cells made of silicon in making solar panels has notable shortcomings such as unaffordability and lack of longevity of the electric power generated. In this regard, therefore, this study purposes to establish ideal photovoltaic properties which increases the durability and efficiency of $\text{CH}_3\text{NH}_3\text{PbI}_3$ solar cells. The purpose of this work was to study computationally the electronic, mechanical and optical properties of $\text{CH}_3\text{NH}_3\text{PbI}_3$ and its potential application in photovoltaic. The specific objectives include determining electronic, mechanical and optical properties of $\text{CH}_3\text{NH}_3\text{PbI}_3$ from first principles and to establish the ideal properties of $\text{CH}_3\text{NH}_3\text{PbI}_3$ for photovoltaic applications. Electronic, mechanical and optical properties of $\text{CH}_3\text{NH}_3\text{PbI}_3$ were calculated using *ab initio* methods specifically Quantum Espresso code. The norm conserving pseudo potential was used. Band gap was calculated as 1.58 eV which is close to the experimental value which is approximately 1.56 eV. Elastic constant parameters such as bulk modulus B , Young's modulus E , shear modulus G and Poisson's ratio ν were calculated using the Voigt–Reuss–Hill averaging scheme. Our calculated lattice parameter a is 6.39 Å comparable to experimental value of 6.33 Å while the Poisson's ratio (ν) in this work is 0.25 and experimental value is 0.28. Optical properties like real (ϵ_1) and imaginary part (ϵ_2) of dependent dielectric function and absorption coefficient were calculated and discussed. The calculated values of all parameters were compared with the available experimental and theoretical values. There is a fairly good agreement between experimental data and this computational work. These findings establish systematic design rules to achieve silicon like efficiencies in a basic $\text{CH}_3\text{NH}_3\text{PbI}_3$ perovskite solar cell.

TABLE OF CONTENTS

DECLARATION	ii
RECOMMENDATION	iii
COPYRIGHT	iv
DEDICATION	v
ACKNOWLEDGEMENT	vi
ABSTRACT	vii
TABLE OF CONTENTS	viii
LIST OF TABLES	xii
LIST OF FIGURES	xi
LIST OF ABBREVIATIONS AND ACRONYMS	xiii
OPERATIONAL DEFINITION OF TERMS	xv
CHAPTER ONE	1
INTRODUCTION	1
1.1 Introduction.....	1
1.2 Background of the Study	1
1.3 Formation of Perovskites Films	4
1.4 Statement of the Problem.....	6
1.5 Purpose of the Study	6
1.6 Objectives of the Study.....	7
1.7 Research Questions.....	7
1.8 Justification of the Study	7
1.9 Scope of the Study	8
1.10 Limitations of the Study	8
1.11 Assumptions of the Study	8
CHAPTER TWO	10
LITERATURE REVIEW	10
2.1 Introduction.....	10
2.2 Solar Spectrum.....	11
2.3 Electronic Structure Properties of Lead Halide Perovskite	13
2.3.1 Band Gap Energy	15
2.4 Mechanical Properties of Lead Halide Perovskite.....	16
2.5 Optical Properties of Lead Halide Perovskite.....	17
2.6 Photovoltaic Cell.....	19

2.6.1 Application of Lead Halide Perovskite in Photovoltaic.....	22
2.7 Density Functional Theory	24
2.7.1 The many-body physics	25
2.7.2 Electronic Density	28
2.7.3 Hartree-Fock Approximation	29
2.7.4 The Hohenberg-Kohn Theorem	30
2.7.5 The Kohn-Sham Equations	31
2.8 Exchange-Correlation Approximations	33
2.8.1 Local Density Approximation.....	33
2.8.2 Generalized Gradient Approximation.....	34
2.9 Plane Wave	34
2.10. Research Gaps.....	36
2.11 Conceptual Framework.....	38
CHAPTER THREE.....	40
RESEARCH METHODOLOGY	40
3.1 Introduction	40
3.1.1 Computational Details.....	41
3.2 Pseudo-Potentials	43
3.3 Relativity and Spin-Orbit Coupling	43
3.4 Energy Cut-off	44
3.5 K-Points	45
3.6 Elastic Constants	46
3.7 The Dielectric Function	48
3.8 Absorption Index and Absorption Coefficient.....	50
CHAPTER FOUR	52
DATA ANALYSIS, PRESENTATIONS AND DISCUSSIONS.....	52
4.1 Introduction.....	52
4.2 Results and Discussions.....	52
4.2.1 Electronic Properties of $\text{CH}_3\text{NH}_3\text{PbI}_3$	52
4.2.2 Mechanical Properties of $\text{CH}_3\text{NH}_3\text{PbI}_3$	58
4.2.3 Optical Properties of $\text{CH}_3\text{NH}_3\text{PbI}_3$	60
4.3 Properties of $\text{CH}_3\text{NH}_3\text{PbI}_3$ for Photovoltaic Application	62

CHAPTER FIVE	66
SUMMARY, CONCLUSION AND RECOMMENDATION.....	66
5.1 Introduction.....	66
5.2 Summary	66
5.3 Conclusion	67
5.4 Recommendation	67
REFERENCES	68
APPENDICES.....	76
Appendix I: Input File for Pwscf Code: Ecut.in, K-points.in and Alat.in.....	76
Appendix II: Input File for Pwscf Code: Pseudo-Cubic Structure	78
Appendix III: Results of Lattice Parameter, Energy, Pressure and Enthalpy	80
Appendix IV: Absorption Coefficient. out.....	81
Appendix V: University Authorization Letter.....	83
Appendix IV: KUREC Clearance	84
Appendix V: NACOSTI Research Permit.....	85
Appendix VII: Publications, Workshops and Conferences.....	87

LIST OF TABLES

Table 1: Calculated lattice parameter (a_0), Bulk modulus B_0 (GPa), derivative of bulk modulus B' and volume (\AA^3) of $\text{CH}_3\text{NH}_3\text{PbI}_3$	53
Table 2: The bond length and bond angle of $\text{CH}_3\text{NH}_3\text{PbI}_3$	54
Table 3: Value of calculated band gap of $\text{CH}_3\text{NH}_3\text{PbI}_3$ in comparison with other studies.....	56
Table 4: Computed elastic constants; C_{11} , C_{12} , C_{44} , Bulk modulus (B), Shear modulus (G), B/G ratio, Young modulus (E), Poisson's ratio (ν) and anisotropy factor (A)	59
Table 5: Comparison of the band gap and absorption coefficient of Silicon and $\text{CH}_3\text{NH}_3\text{PbI}_3$	65

LIST OF FIGURES

Figure 1: (a) Diagram of the pseudo-cubic, (b) tetragonal, and (c) orthorhombic crystals structures of $\text{CH}_3\text{NH}_3\text{BX}_3$ ($\text{B} = \text{Sn}^{2+}, \text{Pb}^{2+}$; $\text{X} = \text{Cl}, \text{Br}, \text{I}$) compounds, respectively. (Feng, 2014)	2
Figure 2: Electromagnetic Spectrum (Verhoeven, 2017)	11
Figure 3: (a) Spectral irradiance of the AM0 spectrum versus photon wavelength (b) photon energy (Gueymard, 2004)	12
Figure 4: Schematic diagram showing direct (a) and indirect band gap (b) transitions (Abedin & Minhaz, 2015).	15
Figure 5: Diagram of PN junction with EV, EF and EC, are the valence band, Fermi level and conduction band energy of the material respectively (Abdussamad Abbas, 2017)	20
Figure 6: PIN and NIP Type (Abdussamad Abbas, 2017)	20
Figure 7: Conceptual Frame work	38
Figure 8: DFT Input and Output	39
Figure 9: Schematic diagram showing the iterative process of solving the Kohn-Sham equation to obtain self-consistent electronic density (Ciucivara, 2007)	42
Figure 10: A graph of Energy against Mesh cut off	45
Figure 11: A graph of total energy verses k-point	46
Figure 12: Total Energy /Cell against Volume of Lattice parameter	52
Figure 13: Crystal structure of $\text{CH}_3\text{NH}_3\text{PbI}_3$ of pseudo-cubic phase	54
Figure 14: Band Structure of $\text{CH}_3\text{NH}_3\text{PbI}_3$	56
Figure 15: Total and partial density of states of pseudo cubic $\text{CH}_3\text{NH}_3\text{PbI}_3$	58
Figure 16: Absorption coefficient against Photon Energy	60
Figure 17: Real $\epsilon_1(\omega)$ and Imaginary $\epsilon_2(\omega)$ part against the Photon Energy	62
Figure 18: Absorption coefficient against photon energy (0 – 6eV)	64

LIST OF ABBREVIATIONS AND ACRONYMS

a_0	:	Lattice constant
α	:	Absorption coefficient
AM0	:	Air Mass Zero
B_0	:	Bulk modulus
B_{VHR}	:	Bulk modulus (Voigt–Reuss–Hill approximation)
Br-	:	Bromide ion
CBM	:	Conduction band Minimum
$CH_3NH_3PbI_3$:	Methyl Ammonia Lead Iodide
CPU	:	Central Processing Time
Cl⁻	:	Chloride ion
Cs⁺	:	Cesium Cation
DFT	:	Density Functional Theory
DMF	:	Dimethyl-formamide
DMSO	:	Dimethyl sulfoxide
DOS	:	Density of states
ϵ	:	Dielectric
Espresso	:	opEn-Source Package for Research in Electronic Structure, Simulation, And Optimization.
EQE	:	External Quantum Efficiency
ECUT	:	Energy cut off
E_{VHR}	:	Young’s modulus (Voigt–Reuss–Hill approximation)
EOS	:	Equation of State
GGA	:	General Gradient Approximation
G_{VRH}	:	Shear modulus (Voigt–Reuss–Hill approximation)
HF	:	Hatree-Fock
I⁺	:	Iodide ion
LDA	:	Local Density Approximation
LSD	:	Local Spin Diodes
LED	:	Light Emitting Diodes
OMHPs	:	Organo-metal Halide Perovskites
PbBr₂	:	Lead (II) Bromide
PbCl₂	:	Lead (II) Chloride

PbI₂	:	Lead (II) Iodide
Pb	:	Lead
PbI₃	:	Tri-iodoplumbate
PCE	:	Power Conversion Efficiency
PDS	:	Photo-thermal deflection spectroscopy
PES	:	Photoelectron Spectroscopy
PBE	:	Perdew-Burke-Ernzerhof
QE	:	Quantum Espresso
QSGW	:	Quasiparticle self-consistent GW theory
SOC	:	Spin Orbit Coupling
SSP	:	Solid State Polymerization
TiO₂	:	Mesoporous
VHG	:	Voigt–Reuss–Hill approximation
VBM	:	Valence Band Maximum
ν_{VHR}	:	Poisson’s ratio (Voigt–Reuss–Hill approximation)
X-CRYSDEN:		X-window CRYstalline Structure and DENsities

OPERATIONAL DEFINITION OF TERMS

Photoelectric Effect: This is the process of emission or ejection of electrons from a metal surface when incident light of sufficient energy is absorbed by a metal surface. The process is also known as photoemission.

Photoelectrons: These are electrons that are ejected from the metal surface by Photoemission.

Photovoltaic Cell: This is any electrical device that converts the energy of light directly into electricity by the effect. It is Also known as solar cell.

Photovoltaic Effect: It is a process that produces voltage or electric current in a Photo voltaic cell when exposed to sunlight.

Photo Voltaic (PV): It is the conversion of light into electricity using Semiconducting materials that exhibit the photovoltaic effect.

Band Gap: The minimum energy that is required to excite an electron from a valence band up to a state in the conduction band where it can

Sunlight: This is a portion of the electromagnetic radiation given off by the sun in particular infrared, visible and ultraviolet light.

Solar Spectrum: It is the spectral distribution which shows the relative weights of individual wavelengths (energy) plotted over all energy

Penetration Depth: It is a measure of how deep light or any electromagnetic Radiation can penetrate into a material. It is defined as the depth at which the intensity of the radiation inside the material falls to $1/e$ (about 37%) of its original value.

Absorption Coefficient: It is how far light of a certain energy or wavelength pass through a material before it is absorbed.

Electronic Properties: It is the ability of a device to conduct the electric current and achieved by studying the microscopic properties as band structure, density of states partial density of states and others

Density of States: It is the number of different states at a particular energy level that electrons are allowed to occupy.

Partial Density of State: It is the relative contribution of a particular atom orbital to the Total Density of states.

Band structure: This describes the range of energy levels that electrons may have within it as well as the ranges of energy that may not have.

Lattice Parameter: This refers to the physical dimension of unit cell in a crystal Lattice.

Mechanical properties: This is the measure of how materials behave under applied forces, reflecting its relationship between its response to and deformation from that applied force they include density, hardness and elasticity.

Bulk Modulus: This is the measure of resistance to volume change due to Compression or application of pressure.

Young's Modulus: It is the ratio of linear stress to linear strain

Shear Modulus: This is the extent of resistance to reversible deformations upon Application of stress.

Poisson's Ratio: It is the approximation of the stability of a crystal contrary to the shear.

Anisotropy: It is the difference, when measured along different axes, in a Material's physical or mechanical properties.

Optical properties: it is defined as the material response to incident radiation and can be described as transmittance, reflectance, refraction, and absorption.

Absorption: Absorption of light is the decrease in intensity of optical radiation as it passes through a material medium due to its interaction with the medium.

Dielectric Function: This describes the response of a material to the application of an alternating electric field.

Real Part: The real part of the dielectric constant describes a material's to interact with an electric field that is store and remit energy without absorbing energy.

Imaginary Part: The imaginary part of the dielectric constant describes a material's ability to permanently absorb energy from a time-varying electric field. Materials with a high imaginary part of the dielectric constant absorbs a lot of electromagnetic energy.

Photoelectric effect: This is the process of emission or ejection of electrons from a metal surface when incident light of sufficient energy is absorbed by a metal surface. The process is also known as photoemission.

CHAPTER ONE

INTRODUCTION

1.1 Introduction

Chapter one is a discussion of the general properties of lead halide perovskites determined through experiments and computational work. The problem that prompted this study was stated, as well as the specific objectives and consequently the research questions which guided the study. The justification and scope of this study was presented as well as the limitations and assumptions made during the research.

1.2 Background of the Study

The general formula of lead halide perovskites is ABX_3 , where A represents an organic positively charged ion ($CH_3NH_3^+$; $CH(NH_2)_2^+$) or an inorganic cation (Cs^+) and X represents a halide such as Iodide (I^-), Bromide (Br^-), or Chloride (Cl^-). The B can be divalent metal ion for example Pb^{2+} , Ge^{2+} , or Sn^{2+} (Zhu & Liu, 2016).

The divalent metal ion gives diverse advantages according to the specific electronic structure, of high electrical mobility, tunable band gap, mechanical and thermal stability, magnetic and dielectric transition, and mechanical plasticity, including structural and functional diversity (Zhang et al., 2018).

The crystal structure of (ABX_3) exists in three phase that is cubic, tetragonal and orthorhombic as studied by Feng (2014). The crystal structure of the three phases is shown in Figure 1.

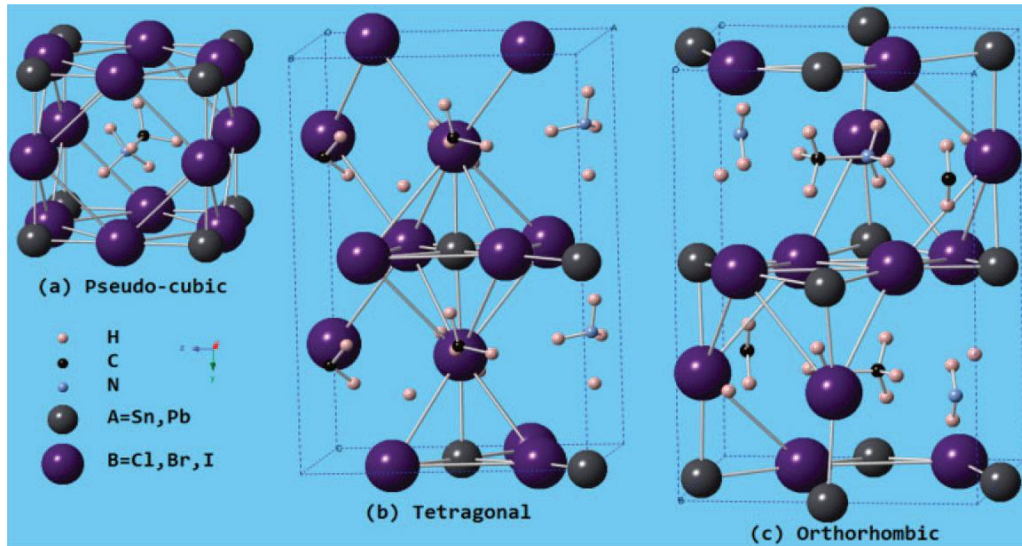


Figure 1:(a) Diagram of the pseudo-cubic, (b) tetragonal, and (c) orthorhombic crystals structures of $\text{CH}_3\text{NH}_3 \text{BX}_3$ ($\text{B} = \text{Sn}^{2+}$, Pb^{2+} ; $\text{X} = \text{Cl}^-$, Br^- , I^-) compounds, respectively.(Feng, 2014)

The structure consists of a network of corner-sharing BX_6 octa-hedra, where the B atom is a metal cation (Sn^{2+} or Pb^{2+}) and X is the hybrid anion (Br^- , Cl^- or I^-). The dependent Octa-hedra gives room for a broad readjustment of the B-X-B bond angle, for this case Pb-I-Pb. The various sets of joint rotations are called tilt transitions (Feng, 2014). This develops symmetry, which shows different structures at varied temperatures. For instant, the three structural phases in which the compound $\text{CH}_3\text{NH}_3\text{PbI}_3$ exist include, pseudo-cubic at increasing temperatures (above 327 K), tetragonal at room temperature, and orthorhombic at reducing temperature (below 162.2 K).

Saliba et al. (2016) stated that lead halide perovskites have become popular as photovoltaic materials due to their high power conversion efficiency (PCE). The PCE of the said perovskites is over 22 per cent. According to Miyata et al. (2017), lead halide perovskites shows great deal of defect tolerance due to their excellent optoelectronic properties. These properties are exhibited by large polarons. An example of lead halide perovskites is the lead bromide perovskites ($\text{CH}_3\text{NH}_3\text{PbBr}_3$) which form a large polaron crystal. One of the attractive properties of these halide perovskites is efficient carrier

transport, manifested by good carrier mobility, long carrier lifetime, and long carrier diffusion length (Du, 2015). The lead halide perovskites are likely not to have mechanistic limitations in relation to charge carrier protection and mobility.

Similar to Saliba et al. (2016) assertion regarding properties of lead halide perovskites, Manser et al. (2016) noted that organic metal halide perovskites constitute a unique group of materials that bridges the gap between low-cost fabrication on one hand, and exceptional device performance on the other hand. The stated compounds are able to be processed at low temperatures usually ranging between 80°C to 150°C . Upon heating, they are able to readily assemble themselves from the thin solution phase into high-quality semi-conductor thin films.

These lead halide perovskites are semi-conducting materials which possess several essential properties. These include low exciton binding energies, long exciton diffusion lengths, high dielectric constants, intrinsic ferroelectric polarization, large absorption coefficients, intense photoluminescence, and also low cost (Lin et al., 2016). It is stated that the fact that these compounds have low energy barriers to crystal formation, the results are both positive and negative. The positive aspect is the inexpensive processing of these perovskites, for both their optical and electronic turn ability. The negative dimension of the perovskites is alluded to the fact that, the thin semi-conductor films formed from many lead halide perovskites lacks both the chemical and structural stability, which makes them to undergo rapid degradation once they get into contact with either moisture or heat (Manser et al., 2016). It is held that the hitherto improvements in solar cells made from lead halide perovskites have been occasioned majorly by the enhanced control over thin film morphology, regulation of the stoichiometry, selected solvent treatment and chemistry of both lead halide and alkyl-ammonium halide precursors (Manser et al., 2016). In this respect, it is averred that effective designing and

co-ordination of processing parameters is bound to facilitate rational optimization of perovskites devices such as solar cells. In the same perspective, the authors recommend various measures that can safeguard the efficiency and durability of the mentioned perovskites devices. The measures include understanding the degradation mechanism of the lead halide perovskites; identifying components of the perovskites structure that is likely to be vulnerable to moisture attack.

1.3 Formation of Perovskites Films

According to Horvath and Miko (1998), the chemical composition of lead halide complexes such as perovskites is adequately established. In relation to this, it is stated that all transition metals which are electronically configured with s^2 , for instance, Sn^{2+} , Pb^{2+} , and SbI^{3+} , readily undergo complexation with halide ions. In the same vein, it is postulated that lead complexes such as tri-iodoplumbate (PbI_3^-), are generally known as plumbates. These plumbates are used as precursors in solutions.

The frequently used solvents for perovskites films formation include dimethylformamide (DMF) and dimethyl sulfoxide (DMSO). These solvents can be able to donate two electrons to lead (Pb), hence forming (Pb^{2+}). When PbI_2 is dissolved in DMSO it turns colourless. However, upon adding excess iodide ions (I^-), it changes from colourless to dark yellow. It is further observed that, replacing solvent ligands with iodide ions, both PbI_3^- and Pb_4^{2-} complexes are formed. These two complexes are characterized by reduced energy charge-transfer absorption bands (Stamplecoskie et al., 2015). According to Manser et al.(2016), the foregoing transformation could be traced easily and also gives greater understanding regarding the occurrences in the precursor solution.

It is noted that, there exists an array of various perovskites precursor formulations that have been developed. These constitute a combination of solvents, halide and molecular ions, and also solvated metals (Manser et al., 2016). It is advisable to be aware of the different interactions which are likely to be manifest among various components. For instance, it is important to understand that the introduction of Cl^- in the precursor combination changes both the solution chemistry and the production progress of the resultant film (Williams et al., 2014).

According to Grancini et al. (2014), most of both physical and optoelectronic properties seen in the end product of the perovskites film is determined by the path followed in the conversion of solution-based precursors to solid-state perovskites. In tandem to this, it is noted that altering the quantitative ratio of $\text{CH}_3\text{NH}_3\text{I}:\text{PbI}_2$ from 3:1 to 1:1 in the precursor solution form thin films with properties that are distinctly different. It is also stated that the spectra of $\text{CH}_3\text{NH}_3\text{PbI}_3$ films deposited from initial ration of 3:1 and the latter ratio of 1:1 precursor solutions on mesoporous Al_2O_3 at different annealing times will differ in absorption and intensity (Manser et al., 2015). The development of spectral features when annealing takes place illustrates the way plumbates complexes are completely changed into perovskites as a result of the organic cation into the lattice. It is further indicated that, in the recent past, solvent chemistry has been explored with the view of improving solution processed perovskites films (Manser et al., 2016). The present study borrows from previous experimental and theoretical studies as it analyses the electronic, mechanical and optical properties of lead halide perovskites computationally.

1.4 Statement of the Problem

The growing need of energy has made it imperative to devise measures of seeking alternative energy sources. One of the crucial alternative sources of electrical energy is solar energy. Silicon based solar cell exhibit various advantages which include; toughness and its stability to high temperature, which have made them suitable materials for photovoltaic applications (Ezealigo et al., 2017). However, the use of the first and second generations solar cells made of silicon has various shortcomings. These include unaffordability and lack of longevity of the electric power generated by the solar energy (Manser et al., 2016). The mentioned attributes, imply that the solar energy so produced is relatively expensive and its sustainability cannot be guaranteed with precision. In this regard, therefore, it becomes imperative to conduct further analysis particularly in respect to third generation solar cells with the view of improving both the durability and longevity of the aforesaid cells. There is limited literature of empirical evidence regarding lead halide perovskites. This necessitates an empirical study to analyse the electronic, mechanical and optical properties of $\text{CH}_3\text{NH}_3\text{PbI}_3$ with respect to its use in photovoltaic. This work studies electronic, mechanical and optical properties with the view of establishing ideal properties for the use as photovoltaic material. It also intends to find ways in which these found properties can enhance durability and efficiency of lead halide perovskite solar cells. The efficiency of solar cells needs practical modelling of fundamental material properties which comprises chemical composition, electronic, mechanical and optical properties (Even et al., 2013).

1.5 Purpose of the Study

The purpose of this work is to determine computationally the electronic, mechanical and optical properties of lead halide perovskite ($\text{CH}_3\text{NH}_3\text{PbI}_3$) and from this, establish the ideal properties for photovoltaic.

1.6 Objectives of the Study

The following specific objectives guided the study;

- i. To determine the electronic properties of $\text{CH}_3\text{NH}_3\text{PbI}_3$ from first principle.
- ii. To compute mechanical properties of $\text{CH}_3\text{NH}_3\text{PbI}_3$ from first principle.
- iii. To study optical properties of $\text{CH}_3\text{NH}_3\text{PbI}_3$ from first principle.
- iv. To establish the ideal properties of $\text{CH}_3\text{NH}_3\text{PbI}_3$ for photovoltaic application.

1.7 Research Questions

The following research questions were addressed;

- i. Which electronic properties of $\text{CH}_3\text{NH}_3\text{PbI}_3$ were determined from first principle and how does these results compare with other work?
- ii. What are the mechanical properties of $\text{CH}_3\text{NH}_3\text{PbI}_3$ determined from first principle and how does these results compare with other work?
- iii. Which optical properties of $\text{CH}_3\text{NH}_3\text{PbI}_3$ were determined from first principle and how does these results compare with other studies?
- iv. What are the ideal properties of $\text{CH}_3\text{NH}_3\text{PbI}_3$ established from the electronic, mechanical and optical properties determined from first principle, for photovoltaic applications?

1.8 Justification of the Study

It is important to conduct this research study due to various reasons. The study is expected to be adequately informative to policy makers in industries that develop solar cells that are or can be made from lead halide perovskites. Our findings should supplement the experimental fabrications of organic solar cells. The results of the study and recommendations thereof will enable researchers to work in adopting the use of lead halide perovskites material in the manufacture of solar panels. The study is further expected to add to the body of knowledge in respect to issues touching on lead halide

perovskites particularly relative to their electronic, mechanical and optical properties. In this regard, therefore, the study will be a source of reference for scholars and researchers in the field of material physics, engineering and related disciplines.

1.9 Scope of the Study

The scope of a study outlines what the study is expected to cover, how, when and where the study is conducted (Kothari, 2004). In regard to the present context, the research focused on computational study of electronic, optical, mechanical properties and the establishment of ideal properties of lead halide perovskite for photovoltaic applications. Quantum Espresso Code was the main code used to facilitate quantum analyses.

1.10 Limitations of the Study

The study faced a number of limitations. There is little research that has been conducted conclusively in relation to electronic, mechanical and optical properties $\text{CH}_3\text{NH}_3\text{PbI}_3$ using computational modelling. This limitation was addressed by comparing the results of this study to findings made in previous experimental and theoretical studies. In this work, QE was used for electronic and mechanical properties and siesta code used as post processing tool for the optical properties.

1.11 Assumptions of the Study

These assumptions include:

- i. Quantum Espresso code would effectively carry out quantum analysis despite the shortcomings associated with this code.
- ii. The time of carrying out the research would be sufficient in coming up with findings that would positively resonate with the study objectives.
- iii. The information and data of previously done work on Lead halide perovskite would be readily available.

- iv. The properties desired could be determined by Quantum Espresso or any other DFT codes and especially optical properties.

CHAPTER TWO

LITERATURE REVIEW

2.1 Introduction

This chapter presents a review of literature pertinent to various properties of lead halide perovskite. The reviewed literature focuses on the solar spectrum, general photovoltaic cell technology, electronic, mechanical and optical properties of $\text{CH}_3\text{NH}_3\text{PbI}_3$ and density function theory (DFT).

The efficiency of the $\text{CH}_3\text{NH}_3\text{PbI}_3$ has increased to more than 22 per cent presently. In 2009, its efficiency rose swiftly from 3.8 per cent to 22.1 per cent in 2016 (Tang et al., 2017). Within a short time, the perovskite solar cells have managed to attain power conversion efficiency of more than or equal to those photovoltaics that have been in use for close to 40 years. Perovskite is cheaper to produce than silicon. Researchers studying and developing the mineral believe that in the future solar panels costing up to 10 to 20 cents per watt will exist. At the moment, the cost of solar panels is usually about 75 cents per watt. Perovskite is also very efficient in absorbing light and has been found to also emit light. It is also noted that it uses less material compared to silicon to absorb similar quantity of light which result to low cost solar power.

Perovskites have a unique structure that makes them ideal for enabling cheap, efficient photovoltaics. Furthermore, Green et al. (2014) stated that its ease in fabrication, strong solar absorption and low non-radiative carrier recombination rates for such simply prepared materials, plus the ability to capitalize on over 20 years of development of related dye-sensitized and organic photovoltaic cells gives perovskite solar cell an upper hand over silicon solar cells. High carrier mobility is a significant property for some cell architectures, as is the range of properties available by forming mixed compounds within a suitable material system. Lattice parameter and crystal structures of $\text{CH}_3\text{NH}_3\text{PbI}_3$

strongly affect the electronic structures such as energy band gaps and carrier transport, which also affects the optical and mechanical properties of the compound. It is for this reason therefore that a detailed analysis of this material and the solar spectrum is necessary.

2.2 Solar Spectrum

All the light coming from the sun is beneficial in one way or another. It comes with varied frequencies. Figure 2 shows the electromagnetic spectrum with variation in frequency, energy and wavelength.

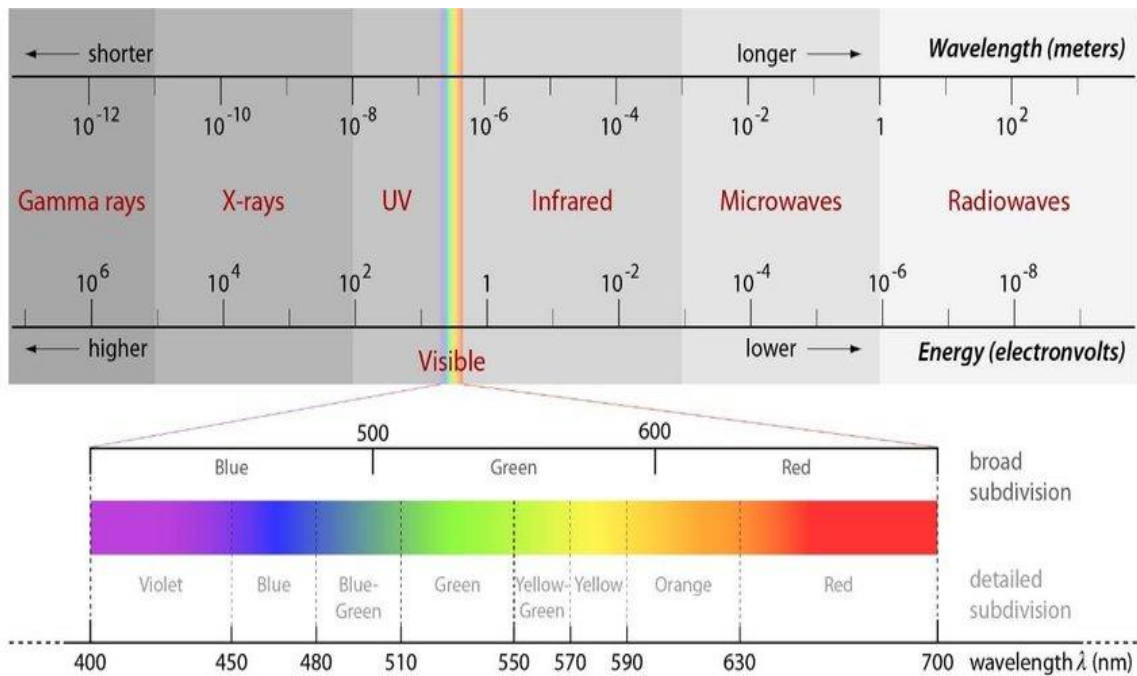


Figure 2: Electromagnetic Spectrum (Verhoeven, 2017)

The useful part of the electromagnetic spectrum in the old generation photovoltaic application is the visible light region. The visible region starts from reduced energy infrared to red, green, blue, violet and increased energy ultraviolet. Silicon solar cell have a band gap energy of 1.2 eV, which is lower that of the red light spectrum. This implies that the greatest part of the infrared light is inadequate to satisfy band gap energy threshold therefore much of the light goes to waste. Band gap is the minimum energy

limit needed to transform solar energy into electricity and the highest permissible energy conversion. For an electron to be excited, it should be supplied with enough energy to meet the band gap energy. The solar energy lower than the band gap energy cannot be absorbed and transformed to electricity.

Infrared contributes 51 per cent of the entire solar spectrum, visible light represent 47 per cent and ultra violet contributes 2 per cent of solar spectrum. The peak is around green and decays for lower and higher frequencies as shown in figure 3 (a).

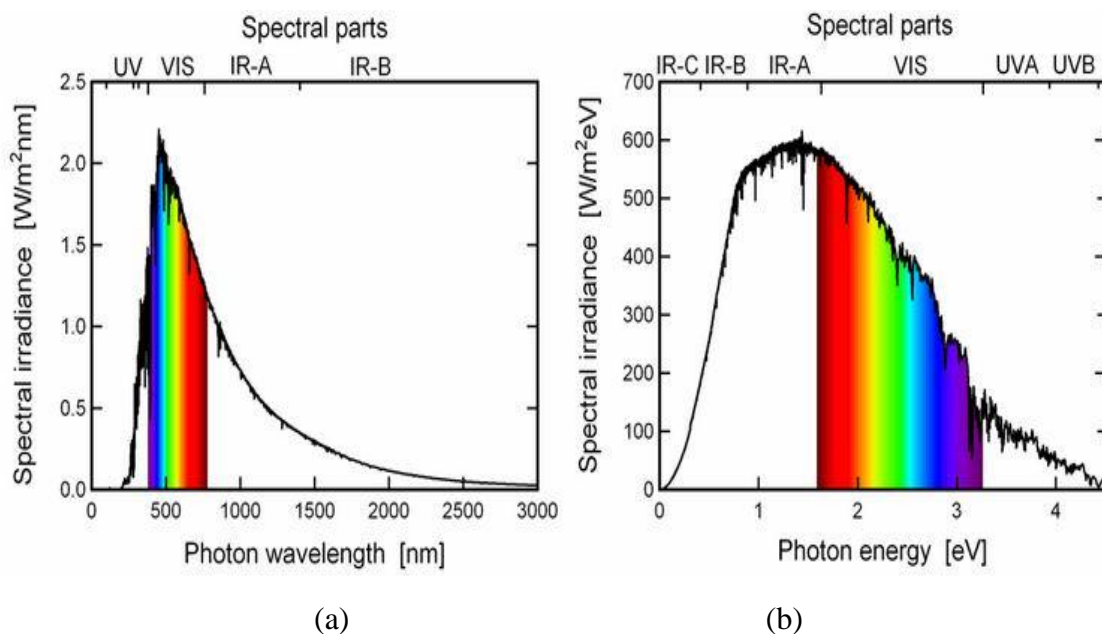


Figure 3:(a) Spectral irradiance of the AM0 spectrum verses photon wavelength (b) photon energy (Gueymard, 2004)

The visible light range wavelength is $\lambda \approx 380\text{--}780$ nm with energy of $\sim 1.6\text{--}3.5$ eV. Photons of light with energy less than 1.6 eV or higher wavelength cannot be absorbed whereas photons with higher energy are instead absorbed (Navaretti, 2018). All the photons with energy lower than the band gap are not utilized, only photons with amount of energy equal to the band gap can be utilized and all the excess energy is wasted in form of lattice vibrations.

2.3 Electronic Structure Properties of Lead Halide Perovskite

A study conducted by Noh et al.(2013) centred on efficiency, chemical management for colourful, and also stable inorganic-organic hybrid nanostructured photovoltaic cell. The results of the study indicated that mixed halide perovskites such as $\text{CH}_3\text{NH}_3\text{PbI}_{3-x}\text{Br}_x$ manifest not only chemical lability which is reduced, but also reduced impact on optoelectronic properties. The study further found that the aforementioned alloys, are known to dissociate once they are irradiated. The findings of this study were supported by a later work of Zhang et al.(2015) on the intrinsic instability of the hybrid halide perovskite semiconductor ($\text{CH}_3\text{NH}_3\text{PbI}_3$).

Phillippe et al. (2015) conducted a photoelectron spectroscopy investigation on the chemical and electronic structure characterization of lead halide perovskites and also their stability behaviour under varied exposures. The study noted that there are hitherto two perovskite materials which have drawn a lot of interest in relation to solar cells. These materials are $\text{CH}_3\text{NH}_3\text{PbI}_3$ and $\text{CH}_3\text{NH}_3\text{PbI}_{3-x}\text{Cl}_x$. The study noted that photoelectron spectroscopy (PES) has the capacity to provide a generalized picture of the electronic structure of the perovskite and the relation of the same to mesoporous TiO_2 when studied with hard X-rays. It was further found that both $\text{CH}_3\text{NH}_3\text{PbI}_3$ and $\text{CH}_3\text{NH}_3\text{PbI}_{3-x}\text{Cl}_x$ exhibit very close electronic structure in spite of having distinct morphologies and kinetics of formation.

A study conducted by Pazoki et al. (2017) analysed the electronic structure of organic-inorganic lanthanide iodide perovskite solar cell materials. The electronic structure of various lanthanide-based materials investigated in the study had not been explored previously in the context of metal-organic halide perovskites. The study revealed that the localized *f*-electrons within the DFT+U approach make the dominant electronic contribution to the states found at the topmost part of the valence band. These results

have a great influence on the photo-physical properties of the lanthanide perovskites. This meant that the primary valence to conduction band electronic transition for MAEul₃ is premised on inner shell F-electron localized states in a periodic framework of perovskite crystals. In different circumstances, the onset of optical absorption would be dormant with respect to quantum confinement effect (Pazoki et al., 2017).

Similarly, Takaba et al. (2017) conducted a study on crystal and electronic structure of substitutive halide perovskites with closer concentration on DFT calculations and molecular dynamics. The study was based on the acknowledgement that the durability of organo-lead halide perovskite is significant due to its practical application in solar cells. The study was guided by density functional theory (DFT) and molecular dynamics to investigate among others, electronic structure of partially substituted cubic MA_{0.5}X_{0.5}PbI₃ (MA = CH₃NH₃⁺, X = NH₄⁺ or (NH₂)₂CH⁺ or Cs⁺). The consequence of pertinent calculation indicated that a partial replacement on MA led to a lattice deformity. Consequently MA or X are prevented from the diffusion between A sites in the perovskite. More so, the computation results from DFT indicated that the electronic structures of the studied partially substituted perovskites were very much identical with that of MAPbI₃. Brivio et al. (2013) obtained the ground state properties of CH₃NH₃PbI₃ using density functional approach. This study outlined the potential energy view, related to the molecular position in pseudo-cubic CH₃NH₃PbI₃. In most CH₃NH₃PbI₃ materials, the valence band maximum (VBM) consists of anti-bonding Pb *s* and I *p* orbitals and the conduction band minimum (CBM) consists of unoccupied Pb *p* orbital. The electronic band gap is within the VBM and CBM. The size of the energy band gap is connected to the maximum voltage in a photovoltaic appliance which is critical in optical absorption.

2.3.1 Band Gap Energy

Band Gap Energy is defined as the minimum energy that is required to excite an electron from a valence band up to a state in the conduction band where it can take part in conduction (Donev et al., 2015). The choice of the appropriate material for trapping sunlight entails obtaining the difference between the value of energy of the valence band energy level and the value of the conduction band energy levels. This gives the band gap energy. The lower-energy valence band is filled with electrons and the high-energy conduction band is often empty. When the photons of light strike the electrons, they absorb sufficient energy to excite them to bounce from the low-energy conduction band into the high-energy valence band. When the electron is in the valence band, its additional energy can then be harvested as electricity.

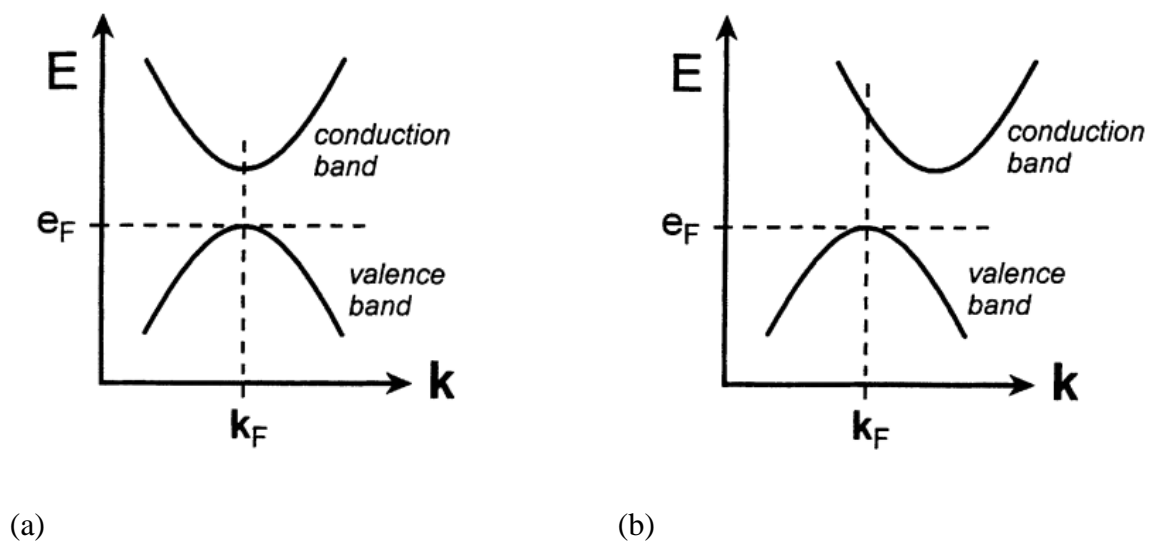


Figure 4: Schematic diagram showing direct (a) and indirect band gap (b) transitions (Abedin & Minhaz, 2015).

There are two types of band gaps that exist, direct and indirect band gaps as shown in figure (a) and (b) respectively. The size and type of this band gap is important since it affects how accurately solar cells transform light into electricity. Electron-hole recombination easily occurs in semiconducting materials with direct band gap since the

valence and conduction band are located directly. Direct band semiconductors are chosen in the fabrication of thin film solar cells and photovoltaic for their high absorption coefficient in comparison with semiconductors with indirect band gaps.

2.4 Mechanical Properties of Lead Halide Perovskite

A study by Feng(2014) investigated the mechanical properties of hybrid organic-inorganic $\text{CH}_3\text{NH}_3\text{BX}_3$ ($\text{X} = \text{Br}, \text{I}; \text{B} = \text{Sn}, \text{Pb}$) perovskites used in photovoltaic cell absorbers. The crystal structures, elastic, and anisotropy properties of the $\text{CH}_3\text{NH}_3\text{PbI}_3$ system were studied using the *ab initio* calculations. The rationale of employing the first-principles (*ab initio*) calculations was premised on the assertion that the mechanical properties of the compounds are relatively difficult to measure through experimental approach. It was revealed that the absorption performance of perovskite solar cell greatly depended on the crystalline and stress state of the perovskite layer. According to Bretschneider et al. (2014), the study concurred with previously done work and it indicated that the mechanical properties of perovskite are crucial for practical applications.

The study conducted by Sun et al.(2017) analysed factors that influence the mechanical properties of formamidinium lead halides and associated perovskites. The study formulated a systematic way of probing the mechanical properties of hybrid perovskite single crystals under nano-indentation. It was revealed that the shape, size and hydrogen bonding resulting from the organic cations occasion significant influence on their mechanical properties. Similarly, it was found that bonding in the inorganic framework and hydrogen bonding play a vital role in determining elastic stiffness. The study also noted that the measured Young's moduli (9.7-12.3 GPa) and hardness (0.36-0.45 GPa) reflected good mechanical flexibility and ductility. The study indicated that the

mechanical properties of lead halide and related perovskites are important in device fabrication and performance.

A DFT study of mechanical properties and stability of cubic methyl-ammonium lead halide perovskites ($\text{CH}_3\text{NH}_3\text{PbX}_3$, $\text{X} = \text{I, Br, Cl}$) was conducted by Faghinasiri et al., (2017). The study was guided by density functional theory. The consolidation of the pseudo potentials PBEsol and vdW type facilitated the determination of the effect of the interaction between PbX_3 scaffold and methyl-ammonium on the mechanical properties of lead halide perovskites. The investigation revealed that the small values of 5.5 per cent applied strains led to the instability of MAPbBr_3 and MAPbCl_3 at room temperature and above.

Moreover, Hu et al. (2017) studied both mechanical and optical properties of Cs_4BX_6 ($\text{B} = \text{Pb, Sn}$; $\text{X} = \text{Cl, Br, I}$) zero dimension perovskites. Specifically, the study investigated the crystal structures, anisotropy, elastic, and optical properties of the aforementioned compounds by employing first-principles calculations. There are two rules which applied to these and other halide perovskites. These are the moduli of Cs_4BX_6 becoming lower in tandem with the order of Cl, Br, and I; and also the moduli of tin-based compounds being larger than lead-based compounds. The study found that Cs_4BX_6 compounds presented definite mechanical anisotropy and also poor ductility.

2.5 Optical Properties of Lead Halide Perovskite

Grancini et al. (2014) conducted a study on how the crystallization procedure effect on the optical and structural properties of hybrid perovskite films for solar cell. Specifically, the study investigated the interrelation between optical and structural properties of organo-lead mixed halide perovskite film as a function of the crystallization process. The results of the study indicated that when methyl-ammonium lead tri-iodide is employed,

the organic cations readjust within the inorganic structure. This results in the organic cations being moved from crystals developed in a mesoporous scaffold to bigger, oriented crystals that are developed on a flat substrate. In effect, there is reduced strain on the bonds forming the structure, thus impacting on the movement of the organic cation within the structure. Ultimately, there is an influence on electronic transformation at the start of the optical absorption spectrum of the semiconductor.

Qarony et al.(2015) conducted an optical scrutiny of $\text{CH}_3\text{NH}_3\text{PbI}_2\text{Cl}$ and $\text{CH}_3\text{NH}_3\text{PbI}_3$ based thin-film perovskite PV cell. Particularly, the study centred on the optics of thin-film smooth surface p-i-n PV cell of organic-inorganic halide perovskites materials. The analysis was premised on the optical wave propagation simulation results of quantum efficiency and short circuit current. The study found that a reference model of PV cell reflects a maximum of 21.8 mA/cm^2 short circuit current and 76 per cent of external quantum efficiency (EQE) when factoring in between 700nm and 620nm of spectral range of wavelengths. It was further observed that $\text{CH}_3\text{NH}_3\text{PbI}_2\text{Cl}$ based solar cell produces 2.7 per cent more short circuit current and approximately 7.5 per cent more proton absorption. This is specifically frequent in regions bordering infrared spectrum regions, which is within wavelengths of 700 nm and 800 nm and for the 360 nm.

The study carried out by Manser et al.(2016) focused on how to make and break lead halide perovskites. The study findings indicated that step-wise solid state transitions from crystalline Solid State Polymerization (SSP) supports with evidence the even transformation of perovskite optical properties when excess alkyl-ammonium halide salt called *vide supra* is used. The results indicate that the formation of perovskite under the stated conditions proceed in tandem with Ostwald's rule of stages (Manser et al., 2016).

A study carried out by Jellicoe et al. (2016) centered on the synthesis and optical properties of lead-free cesium tin halide perovskite nanocrystals. It was found that metal halide perovskite crystal structures constitute optoelectronic materials. This enabled them to merge the ease of solution processing with good optical emission and absorption qualities. The results were in support of earlier findings where solution-processable metal-halide perovskite semiconductors manifested huge potential in optoelectronic appliances like solar cell, lasers and light-emitting diodes (LEDs) [(Lee et al., 2012) and (Jeon et al., 2015)]. These advancements have been occasioned by the excellent optical properties of perovskite which include high photoluminescence quantum yields, sharp absorption edge, and the likelihood of coming up with low-cost device fabrication (Sadhanala et al., (2014) and (Deschler et al., 2014)].

2.6 Photovoltaic Cell

Photovoltaic cell also known as solar cell is a semiconductor used to convert light from the sun to electricity. It should be made of a material that is good enough to trap sunlight energy from sun light. This material is placed amidst two metallic plates that transfers electrical energy produced from light energy to its required destination (Kerr, 2019). Photovoltaic (PV) is the process of conversion of sun light into electricity using semiconducting materials that undergo photovoltaic. Photovoltaic effect is the production of voltage and electric current in an illuminated material.

The photovoltaic cell commonly consists of PN junction as shown in Figure 5.

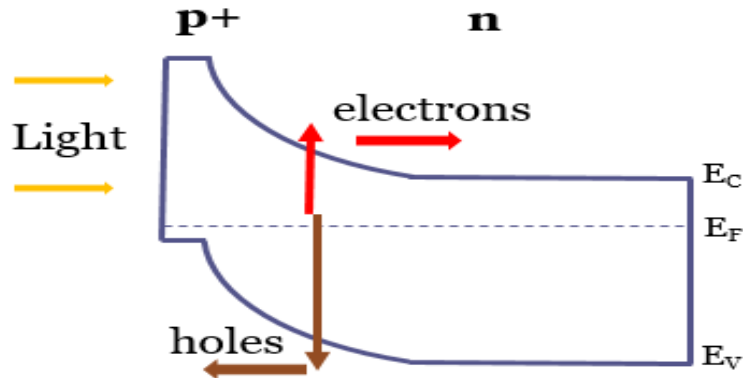


Figure 5: Diagram of PN junction with E_V , E_F and E_C , are the valence band, Fermi level and conduction band energy of the material respectively (Abdussamad Abbas, 2017)

The light penetrating into the solar cell is absorbed and creates electron-hole pairs. These electrons and holes will drift and diffuse, and accumulate on the contacts of a solar cell, which would create a photo-current inside the solar cell, (Abdussamad Abbas, 2017). Solar cells can be made with different structures namely PIN and NIP types.

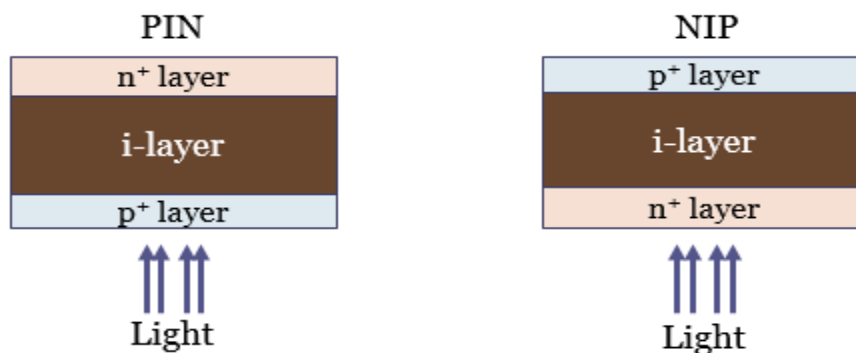


Figure 6: PIN and NIP Type (Abdussamad Abbas, 2017)

The PV cell essential layer is i-layer (perovskite) is put between the p^+ layer and n^+ layer. The distinction between a PIN and a NIP structure is that in PIN structure, light enters from the p^+ side, while in NIP, it enters from n^+ side. Perovskite solar cells can be developed using either PIN or NIP structure. There is a great number of materials that

can be used for p-type layer and n-type layer, (Abdussamad Abbas, 2017). A solar cell (photovoltaic cell) converts solar energy directly into electrical energy by photovoltaic effect, which is a chemical and physical process. A good solar cell must have band gap between 1.0eV to 1.8eV, high optical absorption, high electrical conductivity and abundant availability of raw materials at low cost. The essential parameters of semiconductor that determine the design and the working of a solar cell include;

- Concentrations of doping atoms, which can be of two different types: donor atoms, which donate free electrons and acceptor atoms, which accept electrons. The concentration of donor and acceptor atoms determines the width of the space charge region of a junction.
- The mobility and the diffusion coefficient of charge carriers is used to characterize the carriers transport due to drift and diffusion (Isabella et al., 2014).
- The life-time and the diffusion length of the extra carriers characterize the recombination-generation processes.
- The band gap energy and the complex refractive index, is associated to the absorption coefficient α . Both describe the ability of a semi-conductor to absorb electromagnetic radiation (Isabella et al., 2014). Materials with higher absorption coefficients more easily absorb photons, which excites electrons into the conduction band. The absorption coefficient decides how far into a material, light of a specific energy can infiltrate a material before it is absorbed. For materials with a low absorption coefficient, light is inadequately absorbed. The absorption coefficient rely on the material and also on the light energy being absorbed. Semiconductor materials have a sharp edge in their absorption coefficient, since light which has energy below the band gap does not have enough energy to excite

an electron into the conduction band from the valence band thus, this light is not absorbed.

Some of the mechanical properties of $\text{CH}_3\text{NH}_3\text{PbI}_3$ include elasticity and thermal expansion, which can be determined with the aid of first principles calculations. According to Dong et al. (2017), the calculated full elastic constants facilitate the complete mapping of Young's and shear moduli and also Poisson's ratios along all crystallographic orientations. This helps in assessing the anisotropy of the material. Anisotropy refers to the difference observed when measured along varied axes in a given material's mechanical properties such as refractive index, absorbance, conductivity, and tensile strength.

2.6.1 Application of Lead Halide Perovskite in Photovoltaic.

Ha et al. (2014) investigated the synthesis of organic-inorganic lead halide perovskite nano-platelets with the view of coming up with large performance perovskite PV cells and other electronic and optical appliances. The study observed that highly crystalline organic-inorganic lead halide perovskite nano-platelets grow on muscovite mica where van der Waal epitaxial growth exists. This growth is followed by thermally intercalating methyl ammonium halides.

The findings indicated that the resultant $\text{CH}_3\text{NH}_3\text{PbI}_3$ platelets exhibit great optical properties when diffused with an electron whose length exceeds 200 nm. A study was conducted by Jellicoe et al. (2016) on optical properties of lead-free cesium tin halide perovskite nanocrystals. The study found that despite the fact that the performance of electronics made from perovskites being impressive, the toxicity of the heavy metal component in current perovskite-based devices such as solar cells curtails their large scale prospects. As such, their optical performance notwithstanding, there is

unprecedented interest in replacing lead with other materials that are not toxic. Such materials include bismuth and germanium, whose non-toxicity increases their appeal in solar cells (Marshall et al., 2015). Nevertheless, it is crucial to note that the earlier stated non-toxic materials are not as stable as lead under ambient conditions. This implies that the optical performance of devices made from such non-toxic materials is much lower than their lead-containing analogues (Noel et al., 2014).

According to a study conducted by Hebig et al.(2016) on optoelectronic properties of $(\text{CH}_3\text{NH}_3)_3\text{Sb}_2\text{I}_9$ thin films for photovoltaic applications, the results of solar cell performance were established to be hitherto quite poor. In this study, the absorption properties of the $(\text{CH}_3\text{NH}_3)_3\text{Sb}_2\text{I}_9$ thin film were determined using photo thermal deflection spectroscopy (PDS) measurements on relatively amorphous films. Granted that PDS setup allows the transmitted and reflected light fraction to be measured, an absolute value for the absorption coefficient denoted by α was computed. From the calculations, the study established that high absorption coefficients were in the range of $\alpha > 10^5\text{cm}^{-1}$. The coefficients were deemed to be sufficient for effective light absorption in thin voltaic appliances.

A study by Wang et al.(2016) focused on pressure-induced and optical properties of organo-metal halide perovskite-based formamidinium lead bromide. The study noted that organo-metal halide perovskites (OMHPs) have invoked unprecedented interest as photovoltaic materials associated with moderate cost and important properties. It was further noted that in relation to structural evolution and optical properties of OMHPs, high pressure studies provide crucial hints regarding how to optimize photovoltaic performance. Resultantly, it enables designing of novel OMHPs which have greater stimuli-resistant ability. Similarly, Sun et al.(2017) asserted that hybrid perovskites have

in the recent past drawn a lot of interest as promising materials for photovoltaic and optoelectronic applications.

2.7 Density Functional Theory

A concise description of contents on density functional theory is discussed below;

The theory of Density functional (DFT) came into existence in 1960s. It was developed by Hohenberg, Kohn and Sham and it became known in 1980s. DFT from that time onward has evolved into the main tool for predicting and analysing electronic properties and can also be used in the analysis of mechanical and optical properties of materials. The electronic density distribution in DFT has been thought to be a fundamental property of the many-electron wave function ψ . Presently, there exist various first principle or *ab initio* codes where DFT has been actualized. These codes include periodic, molecular codes, atomic pseudo potential, and DFT functional among others. The electron density calculates the ground state properties. Some examples of *ab initio* codes include Siesta, Yambo, Quantum Espresso, Abinit, Castep and VASP amid other codes. DFT is used because it gives an efficient, but precise quantum mechanical method for physics theorists to optimize structures, compute energies of reactants and products, study the nature of intermediates, and predict the reaction energies for elementary steps (Wang et al., 2014). The theory facilitates determination of many-electron system where functionals are used as manifested in the spatially dependent electron density. The computation codes of DFT are used to investigate the structural, electronic and magnetic properties of molecules, materials and defects. According to Harrison (2001), the density functional theory has been the primary tool used for decades for the quantum mechanical simulation of periodic systems. All properties of a many-particle quantum system may be predicted by finding the solution of the many-particle Schrödinger equation. However, this is expensive computationally since it increases computational cost exponentially with the

number of particles in a system. The main approach for modern electronic-structure calculations is density functional theory, which involves the mapping of many-body quantum system to a single-particle system under an effective external potential.

2.7.1 The many-body physics

Many-body theory (many-body physics) is an area of physics which provides the framework for understanding the collective behaviour of large numbers of interacting particles. On a microscopical examination, a solid is made up of a mixture of protons ion cores in free flowing valence electrons. The ground state electronic properties of a body of this type is seen as bound, isolated system of a number of electrons interacting in an external potential. The configuration of the atomic nuclei creates the external potential, which is sometimes assumed to be fixed point charges. The ion cores consist of nucleus and the inside electrons with full orbitals. The core is considered to be a classical particle since it is large and shift gradually compared to the electrons. The electrons in the valence are smaller and move much faster, therefore treated as quantum particles. They are particularly involved in the bonding process of the solid atoms and are involved in chemical reactions.

The growth in the use of computational codes which uses DFT in Physics is in the initial reorganization of Schrödinger equation to Kohn-Sham equations connected to the knowledge of the correlation effects of interacting electrons in the surrounding of a gradually changing field as stated by (Sifuna et al., 2017). The Hamiltonian for a system is said to contain the kinetic energy T of atoms, the potential energy V or the electron and nuclei interaction energy of the system. Equation. (2.1) gives the many body system Hamiltonian equation;

$$H = \sum_i \frac{-\hbar^2}{2M_i} \nabla_i^2 + \frac{1}{2} \sum_{i,j} \frac{z_i z_j e^2}{(R_i - R_j)} - \sum_k \frac{\hbar^2}{2M_e} \nabla_{rk}^2 + \frac{1}{2} \sum_{k,l} \frac{e^2}{r_k - r_l} - \sum_{k,l} \frac{Ze^2}{r_k - R_l} \quad (2.1)$$

The terms in equation (2.1) are defined as follows;

$$\begin{aligned}
 H = & \sum_i \frac{-\hbar^2}{2M_i} \nabla_i^2 \text{ Represents the kinetic operator for the electrons.} \\
 & + \frac{1}{2} \sum_{i,j} \frac{z_i z_j e^2}{(R_i - R_j)} \text{ Nucleus-nucleus interaction.} \\
 & - \sum_k \frac{\hbar^2}{2M_e} \nabla_{rk}^2 \text{ Kinetic energy operator for nuclei.} \\
 & + \frac{1}{2} \sum_{k,l} \frac{e^2}{r_k - r_l} \text{ Electron-electron interaction.} \\
 & - \sum_{k,l} \frac{Ze^2}{r_k - R_l} \text{ Potential acting on the electrons due to the nuclei.}
 \end{aligned}$$

Where; M_i is the nucleus mass located at R

M_e is the electron mass located at position r_i

Z is the atom's atomic number.

∇ Represents the respective gradients for the terms

R and represents the position of nuclei and electrons, respectively.

Equation. (2.1) can be outlined as in equation (2.2);

$$H = T_e + T_n + W_{en} + W_{ee} + W_{nn} \quad (2.2)$$

From equation. (2.2) T_n and T_e represents the kinetic energy of the nuclei and electrons respectively while W_{en} , W_{ee} , and W_{nn} describes the interaction between electron and nucleus, electron and another electron and nucleus and another nucleus interaction respectively. Finding the solution to equation (2.1) accurately is challenging, because of the many independent variables in the system. Applying the Bohn-Oppenheimer adiabatic approximation in equation. (2.1) can therefore resolve it as mentioned by Zeng et al.(2014). Using the Bohn-Oppenheimer approximation, it is believed that the nucleus is larger than the electronic mass and therefore the movement of the electrons is faster than that of the nucleus. From the adiabatic approximation, the movement of the electrons and that of the ions can be studied independently. This suggests that if the movement of the ions is investigated, then the motion of electrons is ignored and the

converse is true. The total number of wave functions of a system is given as a function describing electrons and other ions.

$$H\psi(\mathbf{R}_1, \dots, \mathbf{R}_N; r_1, \dots, r_n) = E\psi(\mathbf{R}_1, \dots, \mathbf{R}_N; r_1, \dots, r_n) \quad (2.3)$$

From equation 2.3, E represents the system's energy. The sum of E^{el} and E^{nuclei} terms is the total energy E which represents the energy of electrons and nuclei respectively. The variable r_1 and \mathbf{R}_1 are the locations of the electrons and nuclei respectively while N and n are the number of electrons and nuclei of the system respectively.

The Schrödinger equation considers all the interactions within the nuclei and the electron expressed in equation 2.4.

$$\left[-\sum_i \frac{\hbar^2}{2M_i} \nabla_i^2 + \frac{e^2}{2} \sum_{i,j} \frac{1}{(r_{ij})} - \frac{e^2}{2} \sum_{\alpha \neq \beta} \frac{Z_\alpha Z_\beta}{R_{\alpha\beta}} \nabla_{rk}^2 - e^2 \sum_{i,\alpha} \frac{e^2}{|r_i - R_\alpha|} \right] \phi(r_i, R_\alpha) = E_{el}(\mathbf{R}_\alpha) \phi(r_i, R_\alpha) \quad (2.4)$$

In spite of the fact that the problem has been made simple by having the ionic and electronic section, the system continues to have 10^{23} degrees of freedom hence it is still complicated. Considering the quantum many-body problem Schrödinger equation, where W_{en} as the external potential while W_{nn} is taken as a constant but the issue emerges from W_{ee} because the total wave function of all electrons rely on the coordinates of all electrons and therefore difficult to separate them into a single particle problem. This originate from electrons interaction and because of this situation, more advancement is required to do the real system computation. DFT is a good example of the technique used resolve this issue (Manyali, 2014), because the electron density is a variable of only three coordinates and not a wave function that rely on the coordinates of the electrons.

2.7.2 Electronic Density

Taking r_i as the position of electron i with a spin coordinate $\sigma_i = \uparrow$ (spin up) or $\sigma_i = \downarrow$ (spin down) and N as the complete electron electrons. The wave function of the many-electron system defines the quantum mechanical behaviour of the system which relies on the spin and position coordinates $\Psi_e(r_1\sigma_1, r_2\sigma_2, \dots, r_N\sigma_N)$. This wave function according to Ondzibou(2014), fulfils two conditions as stated below;

Condition one is that the wave function has to be normalized,

$$\langle \psi_e | \psi_e \rangle = \sum_{\sigma_1 \dots \sigma_N} \int dr_1 \int dr_2 \dots \int dr_N |\psi_e(r_1\sigma_1, r_2\sigma_2, \dots, r_N\sigma_N)|^2 = 1 \quad (2.5)$$

Condition two, is that it must be anti-symmetric,

$$\psi_e(\dots, r_i\sigma_i, \dots, r_j\sigma_j, \dots) = -\psi_e(\dots, r_j\sigma_j, \dots, r_i\sigma_i, \dots) \quad (2.6)$$

For all electronic systems, the electronic density $n(r)$ for a given state is described as the Number of electrons per unit volume at the point r for that state. The total number of electrons is stated by; $\int n(r) d^3r = N$

The electron density stated as the expectation value of the density is given as;

$$n(r) = \sum_{i=1}^N \delta(r - r_i) \quad (2.7)$$

This in addition imply the relationship between the many electron wave Function and $n(r)$ as;

$$n(r) = N \sum_{\sigma_2 \dots \sigma_N} \int dr_2 \int dr_3 \dots \int dr_N |\psi_e(r_2\sigma_2, r_3\sigma_3, \dots, r_N\sigma_N)|^2 \quad (2.8)$$

The right-hand side of equation (2.8) relates to the wave function normalization integration in equation (2.5) but without one spatial integral, as a result of this one free coordinate left. The electron density $n_\sigma(r)$ is illustrated so that $n_\sigma(r) d^3r$ is the probability to determine the volume element d^3r at r and the electron with spin σ . Integration over the coordinates and spin of the $(N-1)$ other electrons gives,

$$n(r) = \frac{1}{(N-1)!} \sum_{\sigma_2 \dots \sigma_N} \int d^3r_2 \dots \int d^3r_N N! |\Psi(r_1 \sigma_1, r_2 \sigma_2, \dots, r_N \sigma_N)|^2 \quad (2.9)$$

Combining equation(2.5)and (2.9)will yield

$$\sum_{\sigma} \int dr n_{\sigma}(r) = \int (n_{\uparrow}(r) + n_{\downarrow}(r)) = N \quad (2.10)$$

2.7.3 Hartree-Fock Approximation

Hartree-Fock (HF) approximation is a variation technique where the many-electron systems wave functions have the form of an anti-symmetric product of one electron wave functions. HF approximation does not comply with the vital constituent Pauli Exclusion Principle that depends on the many-body wave function to be anti-symmetric in relation to the interchange of two electron coordinates which can be realized by establishing a Slater determinant of single-particle orbitals (Leon, 2008).Consequently it is crucial to add the fermionic nature of the electrons in a many-body wave function so as to make a wave function which is anti-symmetric for the Hartree wave function. This wave function alters the sign when the coordinates of two electrons are exchanged. The Hartree-Fock wave function in form a slater determinant stated as;

$$\Psi^{HF}(r_i) = \frac{1}{\sqrt{N!}} \begin{vmatrix} \Phi_1(r_1) & \Phi_1(r_2) & \dots & \Phi_N(r_N) \\ \Phi_2(r_1) & \Phi_2(r_2) & \dots & \Phi_N(r_N) \\ \vdots & \vdots & \dots & \vdots \\ \Phi_N(r_1) & \Phi_N(r_2) & \dots & \Phi_N(r_N) \end{vmatrix} \quad (2.11)$$

$\Phi(r)$ is given as a one-electron wave function, which is anti-symmetric, under exchange of electrons.

The total energy with the Hartree-Fock wave function is expressed as;

$$E^{HF} = \langle \Psi^{HF} | \hat{H} | \Psi^{HF} \rangle = \sum_i \left\langle \Phi_i \left| -\frac{\hbar^2}{2m} \nabla_r^2 + \hat{V}_{ext}(r) \right| \Phi_i \right\rangle + \frac{e^2}{2} \sum_{ij(j \neq i)} \left\langle \Phi_i \Phi_j \left| \frac{1}{|r-r'} \right| \Phi_i \Phi_j \right\rangle - e^2 \sum_{ij(j \neq i)} \langle \Phi_i \Phi_j | 1/|r-r'| \rangle \quad (2.12)$$

When energy is reduced the variation calculation gives,

$$\left[-\frac{\hbar^2}{2m}\nabla_r^2 + \hat{V}_{ext}(r) + V_i^H(r)\right]\Phi_i(r) - e^2\sum_{j\neq i}\left\langle\Phi_i\left|\frac{1}{|r-r'}\right|\Phi_j\right\rangle\Phi_j(r) = \epsilon_i(r)\Phi_i(r) \quad (2.13)$$

The potential gives the electron-electron interaction in the Hartree-Fock approximation as,

$$V_i^{HF}(r) = e^2\int\frac{n(r')}{|r-r'|}dr' - e^2\int\frac{n_i(r'+n_i^x(r,r))}{|r-r'|}dr', \quad (2.14)$$

Super-cell denotes that the total electron-electron interaction potential is given by

$$V_i^{HF}(r) = e^2\int\frac{n(r')-n_i^{HF}(r,r')}{|r-r'|}dr' \quad (2.15)$$

According to Ondzibou, (2014), the technique created in Chemistry is precise in systems with limited number of electrons.

2.7.4 The Hohenberg-Kohn Theorem

The Hohenberg-Kohn theorem is suitable to any system of interacting electrons subjected to an external potential. The theorem states that; if a system with N interacting electrons is under the influence of an external potential V_{ext} , then a unique ground-state electron density $n(r)$ reduces the corresponding energy functional (Hohenberg&Kohn,1964),

$$E[n] = F[n] + \int n(r) V_{ext}(r) dr. \quad (2.16)$$

Where F is a universal functional of n . Hence the total ground-state electronic energy E_0 is simply the minimum of the functional E . According to (Manyali et al, 2013), a proof of the Hohenberg-Kohn theorem defined a general N -electron functional F as;

$$F[n(r)] = \min_{|\psi\rangle\rightarrow n(r)} \langle\psi|F|\psi\rangle \quad (2.17)$$

Where the expectation value is determined by searching over all N -electron wave functions ψ reducing it to a given density. The selected wave function ψ efficiently reduces the expectation value of F ;

$$\sum_i -\frac{1}{2}\nabla_i^2 + \frac{1}{2}\sum_{i\neq j}\frac{1}{|r_i - r_j|} \quad (2.18)$$

Considering an N-electron ground state wave function ψ_0 yields a density n_0 , then the ground state energy becomes;

$$E_0 = \langle \psi_0 | F + V_{ext} | \psi_0 \rangle \quad (2.19)$$

From equation. (2.19),it's known that

$$F[n_0] = \min_{\psi \rightarrow n_0} \langle \psi | F | \psi \rangle = \langle \psi_{min}^0 | F | \psi_{min}^0 \rangle \quad (2.20)$$

And from the minimum principle

$$F[n_0] + \int V_{ext} n_0(r) d^3r = \langle \psi_{min}^0 | F + V_{ext} | \psi_{min}^0 \rangle \geq E_0 \quad (2.21)$$

Though since

$$F[n_0] = \langle \psi_{min}^0 | F | \psi_{min}^0 \rangle \leq \langle \psi_0 | F | \psi_0 \rangle \quad (2.22)$$

We also have

$$F[n_0] + \int V_{ext} n_0(r) d^3r = \langle \psi_{min}^0 | F + V_{ext} | \psi_{min}^0 \rangle \leq E_0 \quad (2.23)$$

Since ψ_{min}^0 and ψ_0 result to equal density n_0 , therefore from equations. (2.22) and (2.23) implies that

$$E[n_0] = F[n_0] + \int V_{ext} n_0(r) d^3r = E_0 \quad (2.24)$$

Therefore end of proof.

2.7.5 The Kohn-Sham Equations

In Hohenberg-Kohn theorems the precise form of the universal functional F is not known. In order to turn this into a potential scheme Kohn and Sham assumed that the ground-state density $n(r)$ is the density of non-interacting reference system (Kohn& Sham,1965).The functional $F[n(r)]$ is separated into four parts and hence E becomes

$$E[n(r)] = T_s[n(r)] + \frac{1}{2} \iint \frac{n(r)n(r^1)}{|r-r^1|} dr dr^1 + E_{xc}[n(r)] + \int n(r) V_{ext}(r) dr \quad (2.25)$$

Where $T_s[n(r)]$ is the kinetic energy of a non-interacting electron gas with density $n(r)$

i.e.

$$T_s[n(r)] = -\frac{1}{2} \sum_i^N \int \psi_i^*(r) \nabla^2 \psi_i(r) dr \quad (2.26)$$

Equation. (2.25) also defines a general exchange-correlation functional $E_{XC}[n]$. Applying a normalization constraint on the electron density, $\int n(r) dr = N$ one obtains the following variational principle.

$$\frac{\partial}{\partial n(r)} [E[n(r)] - \mu \int n(r) dr] = 0 \quad (2.27)$$

$$\Rightarrow \frac{\partial E[n(r)]}{\partial n(r)} = \mu \quad (2.28)$$

μ is chemical potential. Equation (2.28) which can be written in terms of an effective potential, $V_{\text{eff}}(r)$ and that

$$\frac{\partial T_s[n(r)]}{\partial n(r)} + V_{\text{eff}}(r) = \mu \quad (2.29)$$

Where

$$V_{\text{eff}}(r) = V_{\text{ext}}(r) + \int \frac{n(r')}{|r-r'|} dr' + V_{XC}(r) \quad (2.30)$$

$$\text{With } V_{XC}(r) = \frac{\partial E_{XC}[n(r)]}{\partial n(r)} \quad (2.31)$$

It is worth realizing that non-interacting electrons which move in an external potential

$V_{\text{eff}}(r)$ is described by a ground state density

$$n_0(r) = \sum_{i=1}^N |\psi_i(r)|^2 \quad (2.32)$$

Variation of the $E[n(r)]$ leads to the following one electron Schrödinger equation

$$\left(\frac{1}{2} \nabla_i^2 + V_{\text{eff}}(r) - E_i \right) \psi_i(r) = 0 \quad (2.33)$$

And this set of equations should be solved self-consistently as

$$V_{\text{eff}}(r) = V_{\text{eff}}[n_0(r)] \quad (2.34)$$

In brief, considering a non-interacting reference system, then the equation (2.29) and (2.30) gives a theoretically exact method of obtaining the ground state energy.

2.8 Exchange-Correlation Approximations

Exchange-Correlation Approximation is really a significant scheme in the Kohn-Sham approach. It is denoted as a functional of the density $E_{xc}[n]$. It gives the distinction between the classical Hartree energy and total energy of a system (Sifuna et al., 2017).

This means that;

$$E_{xc}[n] = T(n) - T_0(n) + U_{xc} \quad (2.35)$$

$T(n)$ is the precise Kinetic energy functional, $T_0(n)$ is the non-interacting Kinetic energy functional and U_{xc} is the interaction of the electrons with its own exchange-correlation hole. Using the classical electrostatics interaction amidst the electron density $n(r)$ and the whole density $E_{xc}(r, r')$ we have:

$$E_{xc} = \frac{1}{2} \iint dr dr' \frac{[n(r)n_{xc}(r,r')]}{r-r'} \quad (2.36)$$

The accurate expression E_{xc} is unknown, therefore the approximation functional based on electron density are brought in to represent the term. The exchange-correlation approximate functional discussed in this section are the Local density Approximation (LDA) functional and the Generalized Gradient Approximation (GGA) functional which are commonly used in the first principle calculations.

2.8.1 Local Density Approximation

The local density approximation (LDA) is one of the most important exchange-correlation functional advanced by Hohenberg and Kohn in early 1960s. Through LDA, the exchange-correlation energy functional of DFT only depends on the value of electron density. According to Perdew et al. (1996), the idea was to locally approximate the exchange-correlation energy $E_{XC}[n(r)]$ of an interacting electron system by the exchange-correlation energy of homogeneous electron gas of density $n(r)$, i.e.

$$E_{XC}^{LDA}[n(r)] = \int E_{XC}(n(r)n(r)dr) \quad (2.37)$$

As the earliest exchange-correlation function, LDA has proved to have some weaknesses. It is not able to foretell correctly the magnetic properties of heavy materials and it minimizes the band gap of such material by half or higher.

2.8.2 Generalized Gradient Approximation

The creation of the GGA exchange-correlation functional was the result of an assumption made by Hohenberg and Kohn that LDA would not work in real systems. The findings of Hohenberg and Kohn was further developed by Perdew and co-workers proposing general functional of the type;

$$E_{XC}^{GGA}[n] = \int d^3r f(n, \nabla n) \quad (2.38)$$

Where $E_{XC}^{GGA}[n]$ define the exchange correlation energy. The GGA method gives better results for predicting molecular geometries and ground-state energies, but it is computationally more expensive than LDA. GGA improves LDA by taking into account the gradient of the density in addition to the density at a point.

According to Stampfl and Van de Walle(1999), GGA compared to LDA has generally been found to improve the description of total energies, ionization energies, electron affinities of atoms, atomization energies of molecules. GGA is also reliable for predicting magnetic properties of 3d transition metals. Despite all that success, GGA has its limitations. It fails to predict correctly the lattice parameters and does not accurately treat hydrogen bond. More advanced and probably more accurate than the GGA functional are the new meta-GGA functional like the ones parameterized by Tao-Perdew-Staroverov-Scuseria (TPSS).

2.9 Plane Wave

According to Manyali (2014), computational modelling of solids need a proper definition of unit cell define by vectors a_1, a_2 and a_3 . In crystalline solids, the atoms are mostly

arranged in a regular repetitive pattern. The plane waves are always used because they are treated as the exact Eigen states of the homogeneous electron gas and are neutral specific atom. The Kohn-Sham wave function form of plane-wave expansion is actually suitable for computing the total energy of solids as uses periodicity. Therefore, to solve this single particle Schrödinger equation with a periodic potential and itself periodic and satisfying the Bloch's theorem, the equation is stated as;

$$\psi_{K,j}(r) = e^{ikr} u_{k,j}(r). \quad (2.39)$$

Where the crystal momentum is represented by k and the band index is j . This categorizes the electronic states with the similar k -vector which are described within the first Brillouin Zone. The part $u_{k,j}(r)$ has the periodicity of the crystal and the expansion can be done using a basis set of plane waves.

$$U_{k,j}(r) = \sum_G C_{j,G} + ke^{i(k+G).r} \quad (2.40)$$

The value G is described in the equation $G.b = 2\pi m$, where b is the lattice vectors of the crystal and m represents an integer. The plane-wave expansion is stated as;

$$\psi_{k,j}(r) = \sum_G C_{j,k} + Gke^{ikr} u_{k,j}(r) \quad (2.41)$$

In Bloch states notations, the Kohn-Sham equations is expressed as:

$$\left[-\frac{\hbar^2}{2m}\nabla^2 + V_{eff}(r)\right] \psi_{k,j}(r) = \sum_{k,j} \psi_{k,j}(r) \quad (2.42)$$

$$\text{With } V_{eff}(r) = V_{ext}(r) + V_H(r) + V_{xc}(r) \quad (2.43)$$

And,

$$n(r) = 2 \frac{\Omega_c}{2\pi^3} \sum_j \int_{BZ} |\psi_{k,j}(r)|^2 \Theta(E_F - C_{k,j}) d^3k \quad (2.44)$$

Where V_{ext} , V_H , V_{xc} are correlation potential. Factor 2 in the equation takes into consideration the spin up (\uparrow) and spin down (\downarrow) and Θ is a step function which can be zero

or one. The energy of the highest occupied energy level by single particle is referred to as the Fermi energy E_F and is determined by the number of electrons N_e in the unit cell.

$$\int_{\Omega_c} n(r) d^3r \quad (2.45)$$

Bloch's theorem at every K-point enables the widening of the electronic wave functions in form of discrete set of plane waves. The question of computing unlimited number of electronic states at an unlimited number of K-points broadens in a single unit cell through the use of Bloch theorem. This is an insignificant advancement as it requires numerous number of computations for the distinct K-points. Nonetheless, the electronic states at the K-points are immediate to one another and also identical and for that reason the wave functions can be represented at a single K-point as a region of K-space by the wave function.

2.10. Research Gaps

There are several studies that have been conducted with respect to properties of lead halide perovskite and its photovoltaic applications. Some research done was based on either experimental work or computational studies using (DFT). However, the studies have fallen short of linking the properties to photovoltaic application. (Phillippe et al., 2015) experimentally studied the electronic structure characterization of lead halide perovskites. Pazoki et al.(2017) computationally examined the electronic structure of organic-inorganic lanthanide iodide perovskite solar cell materials. Moreover, (Takaba et al., 2017) theoretically examined the statistic and dynamic properties of partially substituted halide perovskites where MA which can represent (positively charged ion (CH_3NH_3^+ ; $\text{CH}(\text{NH}_2)_2^+$) or an inorganic cation (Cs^+)) are partially substituted by NH_4^+ or $(\text{NH}_2)_2\text{CH}^+$ or Cs^+ on the electronic structure of halide perovskites. Against this

backdrop, however, none of the reviewed studies examined electronic properties of lead halide perovskite and in the context of photovoltaic application of the halide perovskite.

Grancini et al.(2014) examined the connection between optical and structural properties of organo-lead mixed halide perovskite film experimentally. Though the study investigated optical properties, it did not focus on optical performance of lead halide perovskite. A study conducted by Qarony et al.(2015) analysed the optics of organic-inorganic halide perovskites materials in thin-film smooth surface p-i-n PV cell. (Manser et al., 2016) supported the gradual evolution of perovskite optical properties when (vide supra is used. Another study by Jellicoe et al.(2016) examined the synthesis and optical properties of lead-free cesium tin halide perovskite nano-crystals. It is evident, however, that the reviewed studies did not link optical properties to photovoltaic application of lead halide perovskite.

A study conducted by Feng (2014) found that the mechanical properties of perovskite are very significant for practical use. A study conducted by Sun et al.(2017) indicated that the mechanical properties of lead halide and related perovskites are important in device fabrication and performance. Another study by Faghihnasiri et al. (2017) centered on mechanical properties and stability of cubic methyl-ammonium lead halide perovskites. Moreover, Hu et al., (2017) found that Cs_4BX_6 compounds presented definite mechanical anisotropy and also poor ductility. However, the reviewed studies did not examine the effect of mechanical properties on photovoltaic application of lead halide perovskite. The study addressed the identified research and knowledge gaps with respect to properties of lead halide perovskite and photovoltaic application. Some of the research works mentioned above are experimental and others computational (DFT). In this current work we compare its computational results with experimental and previously done computational work to meet the stated objectives.

2.11 Conceptual Framework

This is a diagrammatic representation of study variables and how they are hypothesized to interact. In respect to the proposed study, the conceptual framework is as shown in Figure 7.

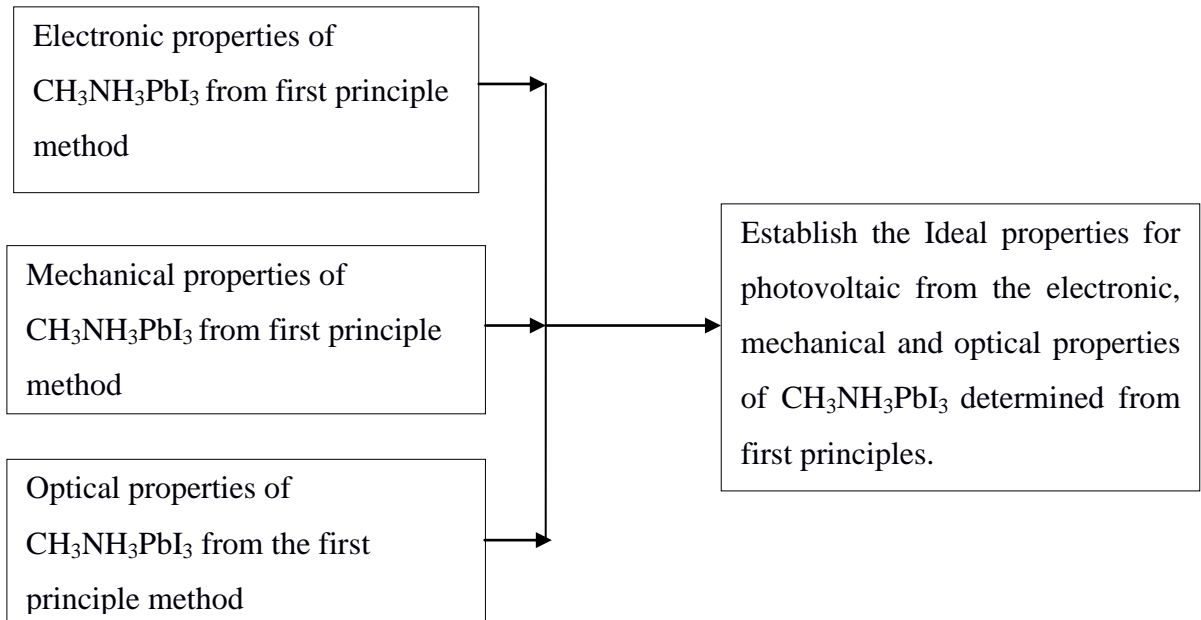


Figure 7: Conceptual Frame work

As illustrated in Figure 7, there are two sets of variables, that is, dependent and independent. Independent variables include electronic properties, optical properties and mechanical properties of lead halide perovskite. Photovoltaic application of lead halide perovskite is the dependent variable. It is hypothesized that the mentioned predictor variables (electronic properties, optical properties, and mechanical properties) influence the photovoltaic application of lead halide perovskite. This general hypothesis guided this study.

Quantum espresso which is one of the DFT codes runs the input file for the different calculations and produces the output which was being determined.

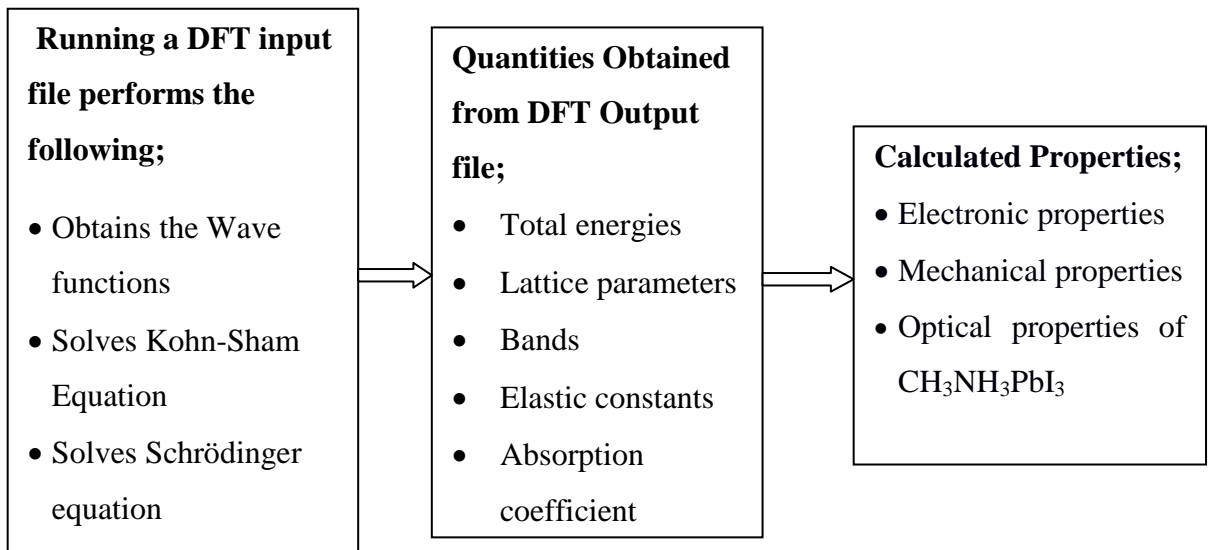


Figure 8: DFT Input and Output

Figure 8 show the various in-built equations that are solved by the DFT code after running input files to obtain the above outputs. The quantities calculated and obtained from the output file were categorized as electronic, mechanical and optical properties.

CHAPTER THREE

RESEARCH METHODOLOGY

3.1 Introduction

Quantum theory gives fundamental understanding and sufficient information on the Physics of materials by simply studying their ions and electrons. This suggests that ions and electrons are important parameters in any quantum mechanical calculations. Using quantum theory, one can be able to differentiate between metals, semiconductors and insulators and characterize them based on their optical, electrical, mechanical and magnetic properties.

The electronic and optical properties of periodic systems are connected to the electronic states defined in the system's electronic band structure. In confined systems like a molecule or an atom in vacuum, the electronic energy levels are quantized by orbitals. In these systems the discrete electronic energy states are uniquely described by four quantum numbers namely; the principal quantum number (n), orbital angular momentum quantum number (l), magnetic quantum number (m) and spin (s) (Azarhoosh, 2017).

This chapter presents an extensive discussion on the methodology, and how the stated specific objectives were met. The entire calculations were performed within the Density Functional Theory and using Quantum ESPRESSO code (Giannozzi et al., 2009) for studying electronic and mechanical properties and Siesta code (Soler et al., 2002) was used as a post processing tool for optical properties. For exchange-correlation functional, the generalized gradient approximation (GGA) was used in quantum espresso and norm conserving pseudo potentials were used for two DFT codes.

3.1.1 Computational Details

Quantum Espresso is an open source code, which can simulate the electrical, mechanical properties and optical properties of a material. For this study we shall use quantum Espresso for electronic and mechanical properties. Quantum Espresso has the following important features applicable to this work.

- a) Ground state calculations based on DFT, Kohn-Sham orbitals.
- b) Structure Optimization (Giannozzi et al., 2009).
- c) QE uses the standard Kohn-Sham self-consistent density functional method in the local density (LDA-LSD) or generalized gradient (GGA) approximations.
- d) Quantum ESPRESSO is based on a plane wave expansion of the electronic wave functions, with a periodic representation of the system in a box under periodic boundary conditions where the box is a primitive cell.
- e) In QE k-sampling of the Brillouin zone, local and orbital-projected density of states, electronic band structure and density of states can be done.

In this work scalar relativistic electronic-structure calculations on this material was done based on density-functional theory (DFT) (Hohenberg & Kohn, 1964), plane waves, and pseudo potentials approach as implemented in the Quantum Espresso computer code (Giannozzi et al., 2009). Exchange and correlation were treated within the Perdew, Burke and Ernzerh of approximation (GGA) (Perdew et al., 1996) to the density functional theory. Core electrons were replaced by *ab initio* norm conserving pseudo potentials, generated using the Troullier-Martins scheme (Troullier & Martins 1991). In the Kleinman-Bylander fully non-local separable representation (Kleinman & Bylander, 1982). These s^1 , $2s^2 2p$, $2s^2 2p^3$, $5s^2 5p^5$ and $5d^{10} 6s^2 6p^2$ were used as valence electrons for H, C, N, I, and Pb respectively. The large overlap between the semi-core and valence states makes it the semi-core 5d electrons of Pb to be treated as valence

electrons and distinctly included in the simulations as explained in Sifuna et al. (2020). In this study, the electronic density, Hartree, and exchange correlation potentials were calculated in a uniform real space grid, with an equivalent plane-wave cut-off of 55 Ry in the representation of charge density. To integrate the Brillouin zone, we employed a Monkhorst-Pack sampling (Monkhorst & Pack, 1976) equivalent to $13 \times 13 \times 13$ in a twelve atom $\text{CH}_3\text{NH}_3\text{PbI}_3$ unit cell (Dalven, 1973).

Figure 9 shows the iterative steps executed in solving the Kohn-Sham equation to obtain a self-consistent electronic density. The iterations are run until the minimum energy desired is attained. This is what constitutes plane waves self-consistent field where the code stops the run after the minimum energy is attained.

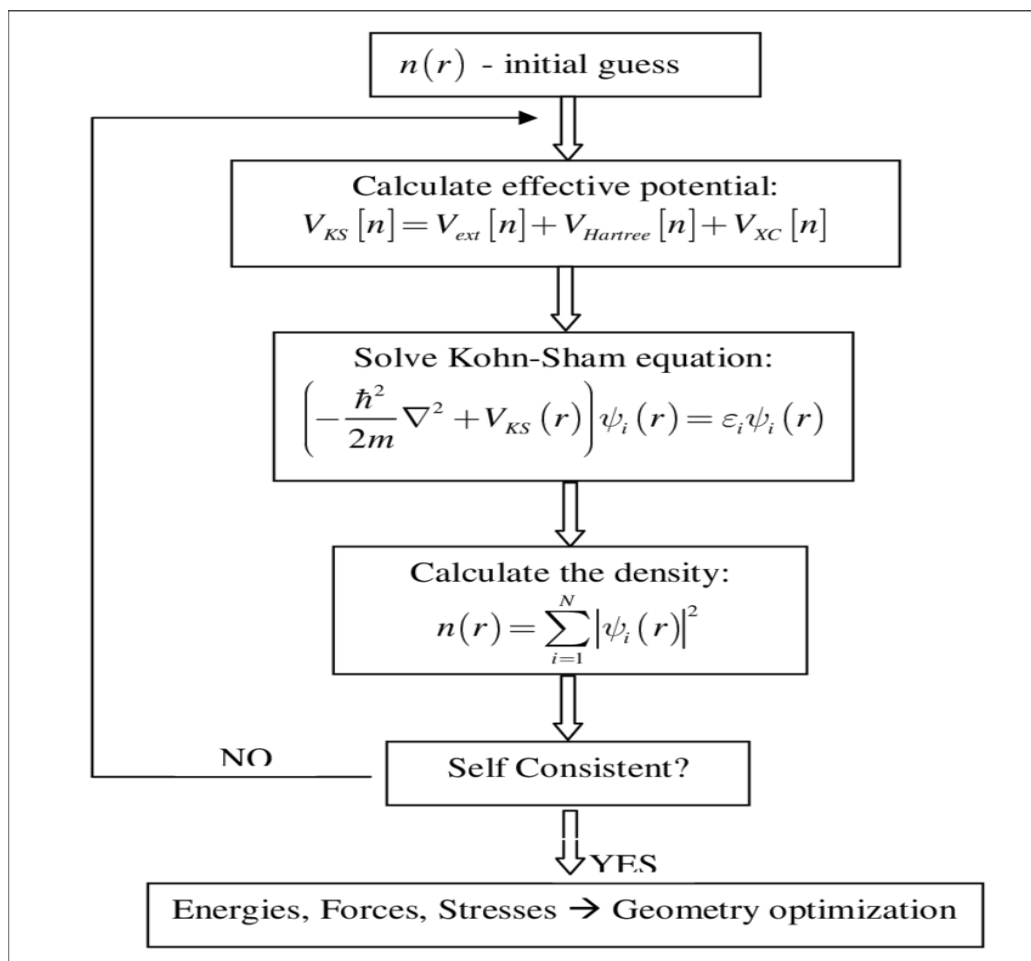


Figure 9: Schematic diagram showing the iterative process of solving the Kohn-Sham equation to obtain self-consistent electronic density (Ciucivara, 2007)

3.2 Pseudo-Potentials

Atoms consist of electrons that is core and valence. The core electrons are localized and their wave functions are not easily expanded within the plane wave basis set. Electrons at the core cannot be overlooked since avoiding them has an effect on the orthogonality within the core and the valence states. The use of pseudo potentials is an approximation which that imitates the core and valence states. Its application in computation has various benefits compared to full potential methods because the cost of computational is minimized. It also ignores the changes of the core electrons and substitutes their effects with an effective potential. There are different classes of pseudo potentials, these classes include; Perdew, Burke and Ernzerhof (PBE), Ultra-Soft and Projector Augmented Wave (PAW) type of pseudo potentials and norm-conserving. In this work, norm-conserving pseudo potentials were used for all the calculations. Both PBE functional and norm-conserving belong to class of generalized gradient approximation (GGA) functional. The outermost *s*, *p*, and *d* electrons in (lead) Pb are taken to be the valence electrons whose interactions with the remaining ions is modelled by pseudo potentials generated within the projector-augmented wave (PAW) (Tao et al., 2017). The total energy convergence in the iterative solution of the Kohn-Sham equations was fixed at 2×10^{-8} Rydberg (Ry).

3.3 Relativity and Spin-Orbit Coupling

Relativistic effects for valence orbitals of light atoms like carbon are normally considered insignificant, yet for heavier atoms like lead (Pb) they can have serious effects (Beltracchi, 2015). Usually, with the critical relativistic effects anticipated for Pb, similar computations have also displayed a major role of spin-orbit coupling (SOC) that greatly lowered the band-gap by inducing a large splitting of the first degenerated conduction levels in the conduction band (Even et al., 2013).

There are two main relativistic effects which are commonly considered when handling solid state systems, that is: scalar-relativistic and spin-orbit. In scalar relativistic effects, the kinetic energy operator in the Hamiltonian is adjusted to involve higher order elements of the relativistic energy expansion, yet the wave function is still considered as a scalar wave function (Capelle, 2006).

The main relativistic effect in perovskite is the spin-orbit interaction which results from magnetic coupling between the varied angular momentum degrees of freedom. The spin orbit inclusion to the Hamiltonian is given by $\Delta H = k\mathbf{S}\cdot\mathbf{L}$, where simply getting the correct form of parameter k involves analysis of the Dirac equation (Sakurai & Napolitano, 2014).

3.4 Energy Cut-off

The convergence test for plane-wave energy cut-off and the k-point grid was determined and the atomic position at fixed lattice constants relaxed at a temperature of 0 K. (Beltracchi, 2015). Volume was varied and atomic coordinates relaxed for every volume. This is a very significant principle in every DFT calculation. The convergence of the energy cut-off in relation to the total energy was determined as follows; A k-point grid was chosen for which the results is expected to be converged, then the system simulated in QE using gradually increasing values of Energy Cut off (ECUT) (Beltracchi, 2015). These ECUT values and their corresponding output values (Energy Ry) was used to plot Figure 10. The figure shows that energy cut-off less than 30 Ry is inadequate. Therefore, to obtain more precise results values greater than 30 Ry should be selected. Greater energy cut-off does not mean precision but it raises the computation cost without tampering with accuracy .It should therefore be averted to cut down the CPU time (Sifuna et al., 2017).

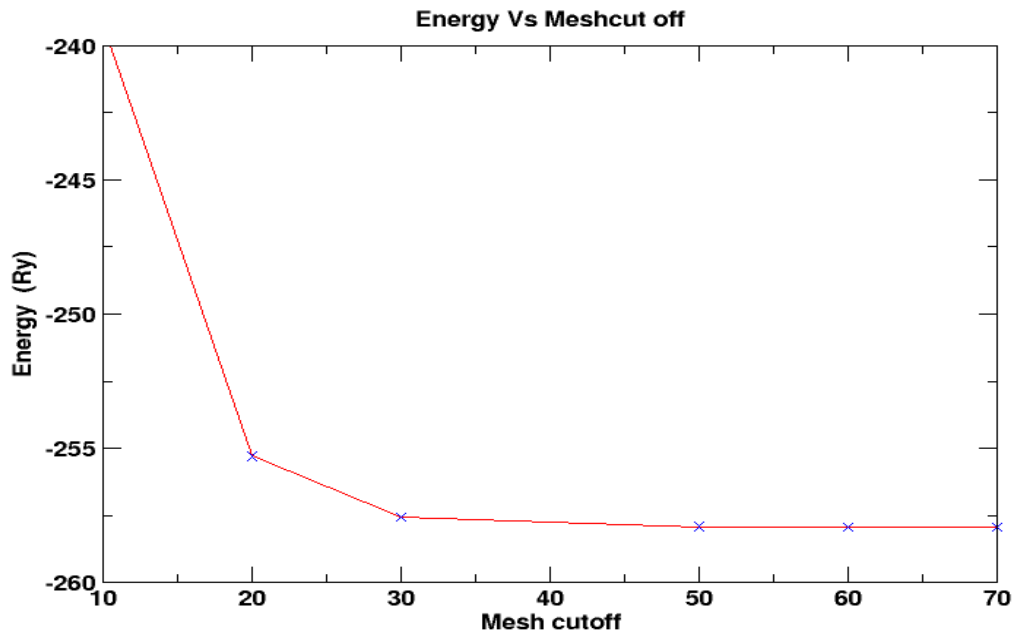


Figure 10: A graph of Energy against Mesh cut off

3.5 K-Points

Weigner-Seitz cell of the reciprocal lattice is the first Brillouin zone. According to Monkhorst and Pack (1976), the frequent method of sampling used in the first Brillouin zone is the evenly spaced Monkhorst-Pack k-point grid. The denser the grid the more the computing power required. A dense grid gives more precise results though one has to decide between accuracy and the computational cost (Sifuna et al., 2017). K-point meshes are to be converged therefore one has to choose carefully the k-points. For this material $\text{CH}_3\text{NH}_3\text{PbI}_3$, a $4 \times 4 \times 4$ k-point grid was found to be sufficient or any value higher than this can be used. According to this work, the graph of energy against K-point size for $\text{CH}_3\text{NH}_3\text{PbI}_3$ illustrated in Figure 11;

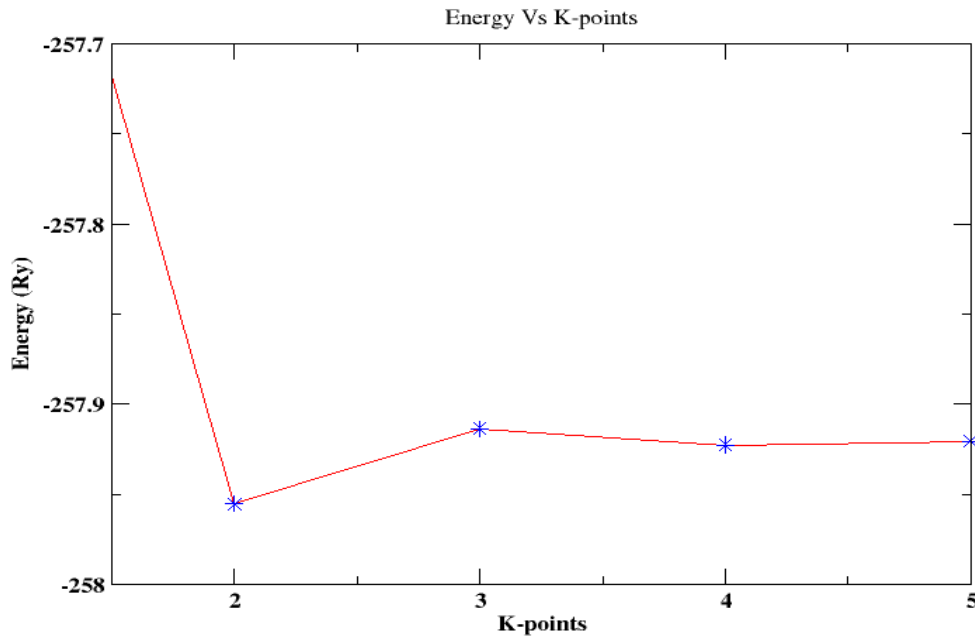


Figure 11: A graph of total energy verses k-point

3.6 Elastic Constants

Mechanical Properties of solids defines components like their strength and resistance to change in shape and size and the capacity of an object to tolerate the stress applied to the object. Mechanical properties of solids include elasticity, strength, abrasion, hardness, ductility, brittleness, malleability and toughness. The elastic constants tell the relation between dynamic properties and mechanical properties concerning forces existing in materials. This gives a lot of importance on the stiffness of a material and its stability (Sifuna et al., 2017).

The elastic constants of a material can also explain its reaction to an exerted stress and give helpful facts concerning its structural stability and bonding character (Leisure, 2004). Furthermore, elastic constants are used to calculate mechanical properties of a material which include the Young's modulus, shear and the Poisson's ratio. The bulk modulus B is the measure of resistance to volume change due to compression or application of pressure. Shear modulus G describes the extent of resistance to reversible deformations upon shear stress. The Shear modulus G and Bulk modulus B were

determined using the Voigt-Reuss-Hill estimation. The Shear modulus G tells how hard a material is. The value of $\frac{B}{G}$ ratio can tell the brittleness and the ductility of a material (Fu, 2008). When the ratio $\frac{B}{G} \leq 1.75$ then a material is said to be brittle and when $\frac{B}{G} > 1.75$ the material is ductile. The ratio of linear stress to linear strain is referred to as Young's modulus E which shows how stiff a material is. Poisson's ratio ν , approximates the stability of a crystal contrary to the shear. Poisson's ratio value is within -1 to 0.5.

According to Ravindran et al. (1998), the Poisson's ratio for ductile materials is $\nu = \frac{1}{3}$ and that for brittle materials $\nu < \frac{1}{3}$. The Poisson's ratio (ν) and Young's Modulus E are connected to the Shear Modulus G and Bulk modulus B by the equations 3.1 and 3.2;

$$E = \frac{9BG}{3B+G} \quad (3.1)$$

$$\nu = \frac{3B-2G}{2(3B+G)} \quad (3.2)$$

The total energy E of a crystal in a strained state is given by equation 3.3;

$$E = E_0 + V_0 \sum_{ij} C_{ij} \sigma_{ij} \epsilon_{ij} + \frac{1}{2} \sum_{ijkl} C_{ijkl} \epsilon_{ij} \epsilon_{kl} \quad (3.3)$$

Where V_0 represents the volume of the unstrained crystal, E_0 represent total energy of unstrained crystal, while E represents its equivalent total energy. $\sigma_{ij} \epsilon_{ij}$ represent an element in the distortion tensor and the indices i, j, k, l run over the plane x, y and z . The simple Cubic $\text{CH}_3\text{NH}_3\text{PbI}_3$ have three autonomous elastic constants C_{12} , C_{44} and C_{11} , which were gotten by putting the total energies in equation 3.3. The Zener anisotropy ratio A is the degree of anisotropy in solids (Ravindran et al., 1998). The value $A=1$ for isotropic material, if $A < 1$ or $A > 1$, then it is used to measure the degree of elastic anisotropy. Equation 3.4 was used to calculate factor A ;

$$A = \frac{2C_{44}}{C_{11}+C_{12}} \quad (3.4)$$

3.7 The Dielectric Function

The dielectric properties of solids are very useful because they bring out the connection between the dielectric properties and the optical properties. The dielectric constant is the ratio of the permittivity of a substance to the permittivity of free space. Permittivity is the degree of a material's ability to store an electric field in the polarization of the medium. For instance, the complex refractive index \tilde{n} is precisely related to the dielectric constant ϵ by the equation;

$$\tilde{n} = \sqrt{\epsilon} \quad (3.5)$$

A dielectric undergoes a polarization that varies linearly with the field, when it is put in an external field. The constant of proportionality therefore determines the dielectric constant. The dielectric constant is basically independent of frequency at lower frequencies, but at particular frequencies called resonance frequencies or inter-band frequencies the atoms in solids absorb energy. These resonances are often in visible region of spectrum or ultraviolet range of frequencies.

The evaluation of the static and frequency-dependent dielectric response functions, such as absorption, reflectance, or energy loss spectra, is crucial in the analysis of the optical properties of bulk semiconductors and metals. It's been broadly acknowledged that an accurate quantitative description needs analysis beyond the independent particle picture. A qualitative harmony between theory and experiment can generally be obtained on the level of DFT i.e., the Kohn-Sham Eigen values and their Eigen functions. Furthermore, the evaluation of the frequency dependent polarizability matrices is crucial for the implementation of most post-DFT schemes, such as GW, (Hybertsen & Louie, 1987) exact-exchange optimized-effective-potential methods, or the Bethe-Salpeter equation

(Sham& Rice, 1966) which constitute the main routes toward a high-level description of the optical properties in extended systems, (Gajdoš et al., 2006).

To study the optical properties of CH₃NH₃PbI₃, the calculation of frequency-dependent dielectric matrix is very important. The frequency-dependent dielectric matrix in the long wavelength limit ($q \rightarrow 0$) can be calculated using the sum over states approach (Gajdoš et al., 2006). The formula for the imaginary part of the dielectric constant is a 3x3

Cartesian tensor

$$\epsilon_2^{\alpha\beta}(\omega) = \frac{4\pi^2 e^2}{\Omega} \lim_{q \rightarrow 0} \left(\frac{1}{q^2} \right) \sum_{c,v,k} 2W_k \delta(\epsilon_{ck} - \epsilon_{vk} - \omega) \times \langle u_{ck+e_{\alpha q}} | v u_{vk} \rangle \langle u_{ck+e_{\beta q}} | u_{vk} \rangle^* \quad (3.6)$$

Where the indices c and v represents the conduction and valence band states, respectively while u_{ck} is the periodic part of the orbitals at the k-point \mathbf{k} . The vector e_{α} are unit vectors for the three Cartesian directions x, y, z axis. The real part of the dielectric constant tensor can be derived from the imaginary part using Kramers-Kronig relations:

$$\epsilon_1^{\alpha\beta}(\omega) = 1 + \frac{2}{\pi} \mathbf{P} \int_0^{\infty} \frac{\epsilon_2^{\alpha\beta}(\omega') \omega'}{\omega'^2 - \omega^2} d\omega' \quad (3.7)$$

Where \mathbf{P} stands for the principle value. The real part of the optical conductivity $\sigma(\omega)$ is stated as

$$\sigma_1(\omega) = R[\sigma(\omega)] = \frac{\omega}{4\pi} \epsilon_2(\omega) \quad (3.8)$$

Where $\sigma(\omega)$ and ω are in the cgs unit of sec^{-1} . The cgs conductivity is 9×10^{11} times greater than the SI conductivity unit (Siemens/cm) given in form of

$$\sigma_1(\omega) = \frac{\epsilon_2(\omega) \cdot \omega}{60} \quad (3.9)$$

Where ω is in the unit of cm^{-1} . The corresponding imaginary part of $\sigma(\omega)$ in SI unit is (Tanner, 2016)

$$\sigma_1(\omega) = -\frac{\omega(1 - \epsilon_1(\omega))}{60} \quad (3.10)$$

The complex dielectric constant can be expressed as:

$$\varepsilon(\omega) = \varepsilon_1(\omega) + i\varepsilon_2(\omega) = \frac{4\pi i}{\omega} \sigma(\omega) = (\tilde{n} + i\tilde{k}) \quad (3.11)$$

Where \tilde{n} and \tilde{k} are the index of refraction and the extinction coefficient respectively, and can be evaluated by the computed dielectric constants from equations (3.5) and (3.6)

$$\tilde{n} = \frac{1}{\sqrt{2}} (\varepsilon + (\varepsilon_1^2 + \varepsilon_2^2)^{\frac{1}{2}})^{\frac{1}{2}} \quad (3.12)$$

$$\tilde{k} = \frac{1}{\sqrt{2}} (-\varepsilon_1 + (\varepsilon_1^2 + \varepsilon_2^2)^{\frac{1}{2}})^{\frac{1}{2}} \quad (3.13)$$

The normal incidence, the reflectivity R and the absorption coefficient α (sec^{-1} in cgs unit) in terms of \tilde{n} and \tilde{k} are defined as (Tanner, 2016)

$$R = \frac{(\tilde{n}-1)^2 + \tilde{k}^2}{(\tilde{n}+1)^2 + \tilde{k}^2} \quad (3.14)$$

$$\alpha = \frac{2\omega\tilde{k}}{c} \quad (3.15)$$

The SI unit of ω and α are in cm^{-1} , $\alpha=4\pi\omega\tilde{k}$. In all cases, both the low frequency region $\omega\tau \ll 1$ (τ is the relaxation time) and the high frequency region $\omega\tau \gg 1$ are widely studied to investigate the exact ground state of the material as the two regions carry the signatures of two specific mechanisms associated with optical conductivity in a solid. While the low frequency region is dominated by free carriers which are in abundance in a metal, the high frequency region is dominated by inter-band electronic transitions typical of a dielectric material. As in the limit $\omega\tau \ll 1$, both \tilde{n} and \tilde{k} become sufficiently large, for example, in a metallic conductor,

$$R = 1 - \frac{2}{\tilde{n}} \rightarrow 1 \quad (3.16)$$

This means that the conductor is characterized by its behaviour as a perfect reflector with an exceedingly large absorption coefficient in the low frequency region.

3.8 Absorption Index and Absorption Coefficient

Absorption index is measure of the attenuation caused by the absorption of energy per unit of distance that occurs in an electromagnetic wave of given wavelength propagating in a propagation medium of given refractive index.

The value of the absorption index is given by the relation

$$K = \frac{\alpha\lambda}{4\pi n} \quad (3.17)$$

Where K represents the absorption index, α is the absorption coefficient, λ is the wavelength in vacuum, and n is the refractive index of the absorptive material, i.e., the propagation medium (Weik, 2000).

The absorption coefficient α , tells how far light of a certain energy or wavelength pass through before it is absorbed. It is given by;

$$\alpha = \frac{4\pi kn}{\lambda} \quad (3.18)$$

Materials with a low absorption coefficient, have poor light absorption ability. The absorption coefficient rely on the material and the wavelength or energy of light which is being absorbed. Semiconductor materials possess a critical absorption coefficient, since light with energy below the band gap does not have adequate energy to excite an electron into the conduction band from the valence band, therefore such light is not absorbed (Christiana & Stuart, 2019).

The absorption coefficient shows that the light intensity decreases as the light is absorbed into material. It can be expressed as Beer-Lambert law;

$$I = I_0 e^{-\alpha x} \quad (3.19)$$

Where I_0 , x , α and I are the initial light intensity, the thickness of the material, absorption coefficient and amount of photons after the absorption respectively, (Nelson, 2003). In the next chapter discussion of the outcome of this work is presented in detail. Electronic structure, mechanical properties and optical properties are presented. These properties are then connected to photovoltaic applications.

CHAPTER FOUR

DATA ANALYSIS, PRESENTATIONS AND DISCUSSIONS

4.1 Introduction

In this chapter, results, presentation of data and discussion of electronic, mechanical properties and optical properties of $\text{CH}_3\text{NH}_3\text{PbI}_3$ with regard to the ideal properties of photovoltaic cell are presented.

4.2 Results and Discussions

4.2.1 Electronic Properties of $\text{CH}_3\text{NH}_3\text{PbI}_3$

The resulting total energies of the system and the volumes of the unit cell were applied to the Murnaghan Equation of State (EOS) (Murnaghan, 1944), to get the equilibrium Volume and bulk modulus, as illustrated in Figure 12.

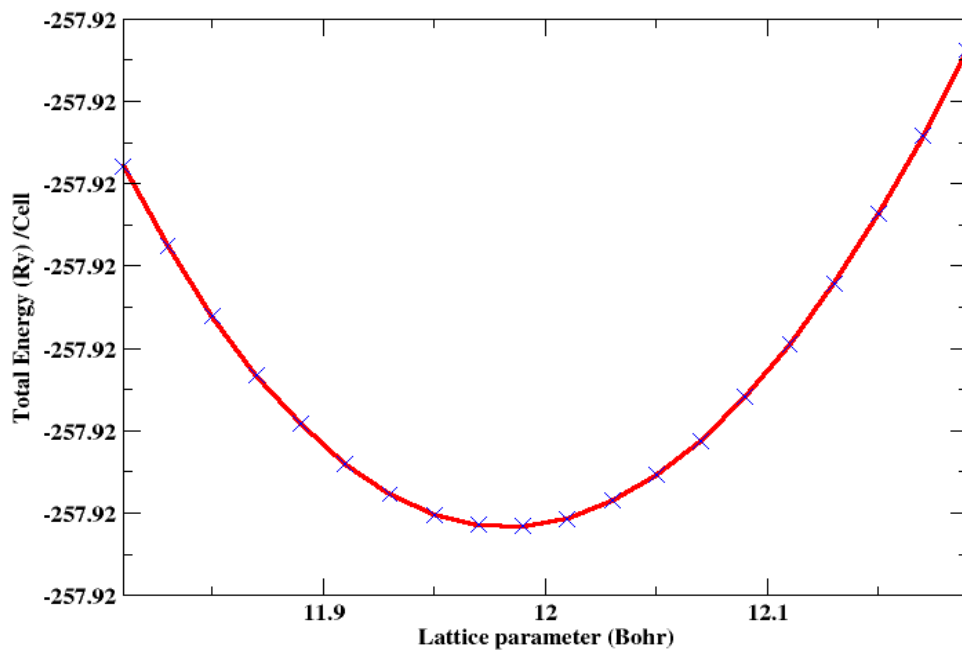


Figure 12: Total Energy /Cell against Volume of Lattice Parameter

Lattice constant tests were performed to obtain relaxed pseudo cubic structure as shown in Figure 12 with optimized lattice parameter being 6.39Å which is equivalent 12.08 Bohr. The bulk modulus B_0 and derivative of bulk modulus B' was found to be 43.31GPa and 17.13 respectively.

Table 1 shows results of calculated lattice parameter of $\text{CH}_3\text{NH}_3\text{PbI}_3$ in comparison with other studies. Lattice parameter was obtained as 6.39Å which agree with other results.

Table 1: Calculated lattice parameter (a_0), Bulk modulus B_0 (GPa), derivative of bulk modulus B' and volume (Å^3) of $\text{CH}_3\text{NH}_3\text{PbI}_3$.

	$a(\text{Å})$	$B_0(\text{GPa})$	B'	Volume (Å^3) ³
This work	6.39	43.31	17.13	260.92
Stoump et al. (2013)	6.31	-	-	251.240
Brivio et al.(2013)	6.46	-	-	269.586
Feng(2014)	6.31	16.4	-	251.240
Brivio et al.(2014)	6.28	-	-	247.673

According to Dalven (1973), the relative energy gap (E_0)is inversely proportional to the square of the lattice constant (a_0)²:

$$E_0 \propto \frac{1}{(a_0)^2} \quad (4.1)$$

Zekry (2017) stated that when value of the lattice constant is decreased the inter-atomic distance will be reduced. As a result, the binding forces between the valence electrons and the parent atoms will increase. The valence electrons in the valence band are bound and for them to become conduction electrons they have to be supplied with energy to make them move freely inside the material. The minimum energy that must be added to valence electrons to be a conduction electron is the energy gap. As the valence electrons

get more bound by reducing the inter-atomic distance, the more the energy required to make them free in the conduction band. Obtaining the appropriate lattice parameter is therefore important so as to get a suitable band gap.

A pseudo cubic phase structure of $\text{CH}_3\text{NH}_3\text{PbI}_3$ was modelled and viewed in x-Crystden as shown in Figure13. The input file in Appendix II was used to draw figure 13.

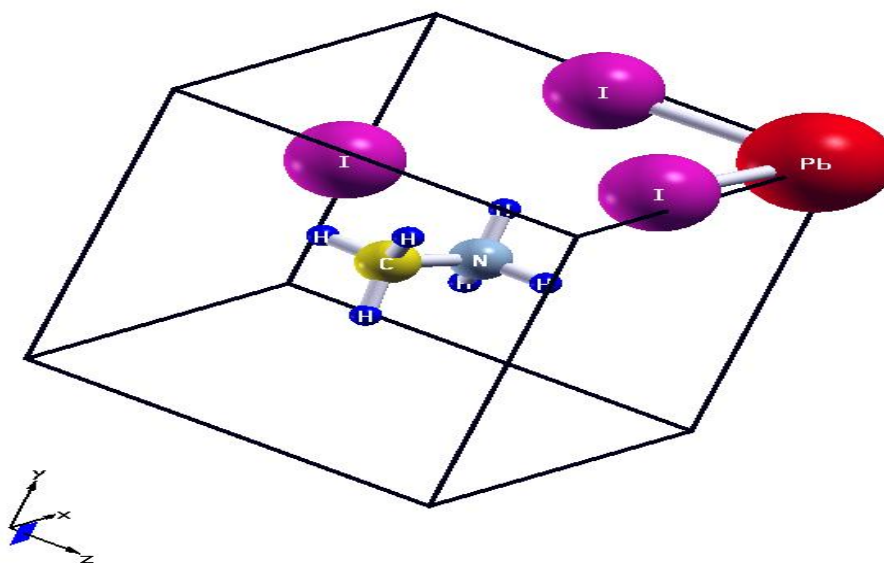


Figure 13: Crystal structure of $\text{CH}_3\text{NH}_3\text{PbI}_3$ of pseudo-cubic phase

The bond angle and bond length obtained from figure 13 are shown in Table 2.

Table 2: The bond length and bond angle of $\text{CH}_3\text{NH}_3\text{PbI}_3$

	Bond length (Å)		Bond angle(°)
Pb-I	3.26	I-Pb-I	79.83 ⁰
N-H	1.20	H-N-H	107.21 ⁰
C-N	1.49	H-C-H	110.37 ⁰
C-H	1.12	-	-

According to Dang et al. (2015), the bond length Pb-I and bond angle I-Pb-I was obtained as 3.1637 Å and 89.988⁰ respectively. These values closely compare with results obtained from this study.

The bond length is the distance between the centres of the two kinds of atoms. The bond length is known to be twice the lattice parameter Berger (2017). Considering the bond length between I-Pb-I atoms since it is along the unit cell, twice the bond length 3.26\AA gives 6.52\AA . This is close to the calculated value 6.39\AA .

The size of the electronic band gap of a material is very critical for it to be used as solar cell absorber since an appropriate band gap is required in the absorption of the photons located in the infrared region of the solar spectrum. The nature of the band gap assists in the estimation of the amount of light absorbed in maximizing the efficiency of the solar cell (Mayengbam et al., 2018).

The efficiency of a solar cell therefore depends on the band gap of the material. It is for this reason that the electronic properties of $\text{CH}_3\text{NH}_3\text{PbI}_3$ are investigated with an aim of improving its efficiency as a solar cell material. In this study, the band gap of optimized structures of $\text{CH}_3\text{NH}_3\text{PbI}_3$ was approximated from the band structure in figure 14. The calculated electronic band gap of the optimized $\text{CH}_3\text{NH}_3\text{PbI}_3$ was found to be 1.58 eV, which is comparable with results from other studies. The comparative results are shown in Table 3. Calculating the band gap considering the SOC affects its size, since it lowers the band gap by inducing a large splitting of the first degenerated conduction levels in the conduction band (Even et al., 2013). This was however not considered in this work.

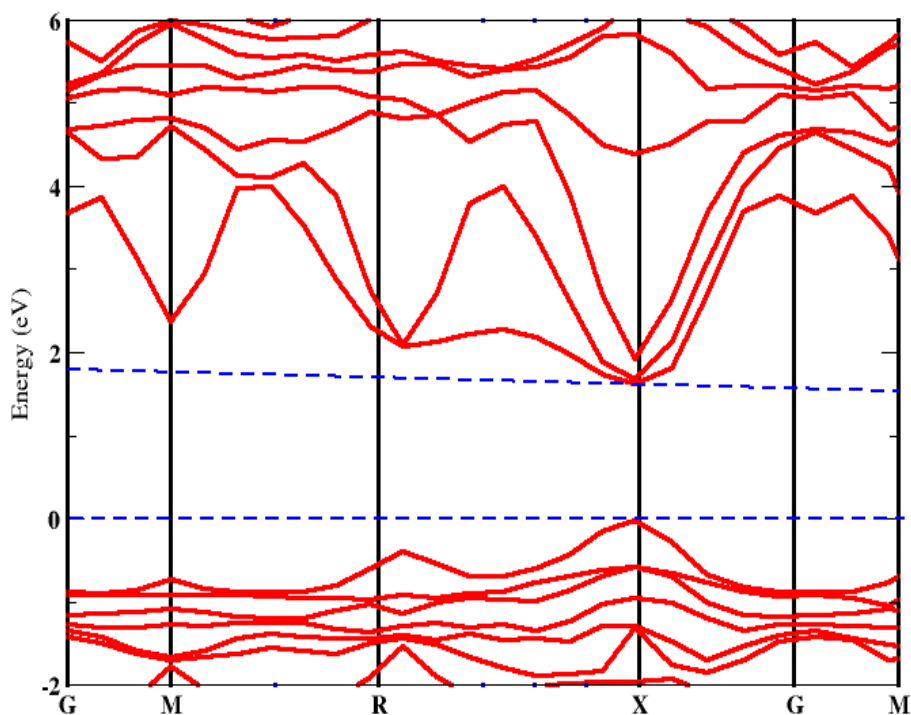


Figure 14: Band Structure of $\text{CH}_3\text{NH}_3\text{PbI}_3$

It was observed from figure 14 that the band gap is direct at the point X with the top of the valence band and the conduction band dominated by iodine orbitals. The Pb 6s, Pb 6p, and I 5p orbitals lie along the X symmetry of figure 14, which is shown clearly in figure 15. The direct gap is suitable for photo absorption since it is a signature for most optical materials.

Table 3: Value of calculated band gap of $\text{CH}_3\text{NH}_3\text{PbI}_3$ in comparison with other studies

Research Done	Band Gap
This work	1.58 eV QE
Brivio et al.(2014)	2.73eV QSGW
Noh et al.(2013)	1.50 Experimental
Yamanda et al. (2014)	1.61 Experimental
Wang et al. (2013)	1.71eV PBE
Kanhere et al. (2015)	1.65 CASTEP

The band gap obtained was found to be close to the experimental value by Noh et al.(2013)and Yamanda et al. (2013) shown in table 3.The band gap 1.58 eV obtained by QE from this work was found to be less than 2.73 eV Brivio et al. (2014) obtained by quasi particle self-consistent GW theory (QSGW)which was found to be an over estimate. According to Brivio et al.(2014) the theory and experiment cannot be compared to better than 0.1 eV resolution for a number of reasons. The experimental band value has been noted to be affected by temperature because of the material structural flexibility which is yet to be investigated (Brivio et al., 2014).

As stated by Prasanna et al. (2017) the *ab initio* calculation of the electronic band structure indicates that VBM of ABX_3 group of metal halide perovskites is an anti-bonding hybrid state of the metal **s** and halide **p** orbitals, while CBM is a hybrid of metal **p** and halide **p** orbitals with lower anti-bonding and greater non-bonding type (Prasanna et al., 2017). Brivio et al. (2013) mentioned that, in most $CH_3NH_3PbI_3$ materials, the valence band maximum (VBM) consists of anti-bonding Pb *s* and I *p* orbitals and the conduction band minimum (CBM) consists of unoccupied Pb *p* orbital.

This is confirmed in the PDOS shown in Figure 15.

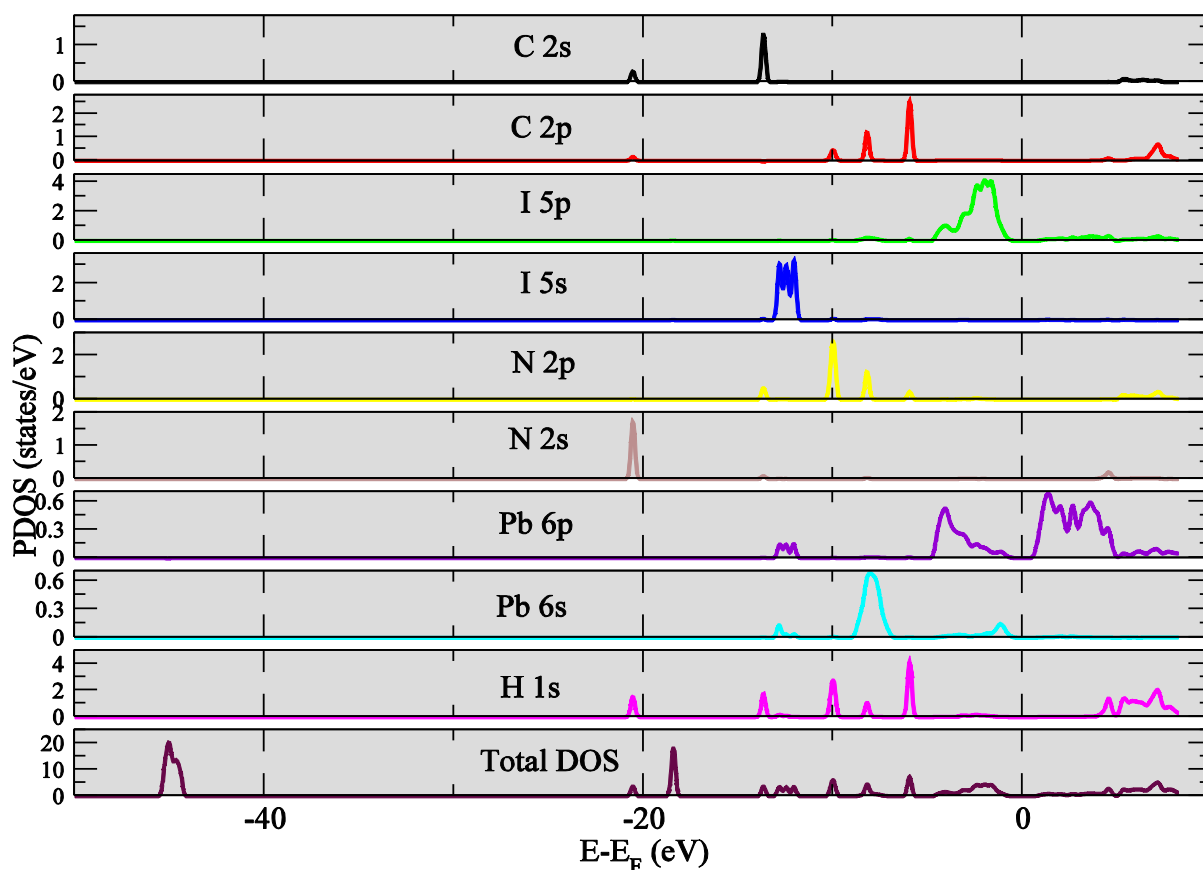


Figure 15: Total and partial density of states (PDOS) of pseudo cubic $\text{CH}_3\text{NH}_3\text{PbI}_3$

Figure 15 shows the orbital contribution of $\text{CH}_3\text{NH}_3\text{PbI}_3$ to the band structure. The Density of states (Dos) is decomposed into the main electron states of each component, the vertical line at 0-point denotes the Fermi-level.

The band edge states are dominated by (PbI_6) anion group in $\text{CH}_3\text{NH}_3\text{PbI}_3$, the group $(\text{CH}_3\text{NH}_3)^+$ does not directly participate in the construction of the bond edge states but indirectly influences the structural and electronic level through Jahn-Teller effect (Meng et al., 2018).

4.2.2 Mechanical Properties of $\text{CH}_3\text{NH}_3\text{PbI}_3$

Mechanical properties of solids include elasticity, strength, abrasion, hardness, ductility, brittleness, malleability and toughness. The elastic constants tells the relation between

dynamic properties and mechanical properties concerning forces existing in materials. The elastic constants of $\text{CH}_3\text{NH}_3\text{PbI}_3$ determined in this work are given in Table 4.

Table 4: Computed elastic constants; C_{11} , C_{12} , C_{44} , Bulk modulus (B), Shear modulus (G), B/G ratio, Young modulus (E), Poisson's ratio (ν) and anisotropy factor (A)

	This work	Computational results Feng(2014)
C_{11}	26.87	27.1
C_{12}	8.6	11.1
C_{44}	10.57	9.2
B	15.8	16.4
E	20.6	22.2
G	7.6	8.7
ν	0.25	0.28
B/G	2.08	1.89
A	0.6	-

Table 4 shows the mechanical properties calculation of the $\text{CH}_3\text{NH}_3\text{PbI}_3$ using Quantum espresso code and results compared with other available data. The results show that our calculated elastic constants for $\text{CH}_3\text{NH}_3\text{PbI}_3$ compare well with other work. These results confirm that pseudo cubic $\text{CH}_3\text{NH}_3\text{PbI}_3$ is stable mechanically because it fulfilled the Born stability criteria of cubic crystals whereby $C_{44} > 0$, $C_{11} > C_{12}$ and $C_{11} + 2C_{12} > 0$ (Mouhat & Coudert, 2014). The ratio $\frac{B}{G}$ obtained was found to be greater than 1.75 implying that $\text{CH}_3\text{NH}_3\text{PbI}_3$ is a ductile material (Fu, 2008).

The computed anisotropic ratio which was gotten as 0.6 indicated that cubic $\text{CH}_3\text{NH}_3\text{PbI}_3$ was elastically anisotropic because substituting it in equation 4.5 it was obtained to be smaller than one ($A < 1$). The Poisson's ratio obtained was 0.25 which when rounded off to one decimal place is closely equal to 0.3 Pugh (1954) which confirms that $\text{CH}_3\text{NH}_3\text{PbI}_3$ is a ductile material.

4.2.3 Optical Properties of $\text{CH}_3\text{NH}_3\text{PbI}_3$

Optical properties of material include reflectance, conductivity, absorption, refraction, transmittance, dispersion, diffraction and so on. The main optical property studied in this work with respect to its suitability as a photovoltaic material is the absorption ability of $\text{CH}_3\text{NH}_3\text{PbI}_3$ therefore absorption coefficient was determined.

4.2.3.1 Absorption Coefficient

The absorption coefficient calculates how deep light rays will penetrate into a layer before it is absorbed. Light is rarely absorbed in a material with a low absorption coefficient. For a direct gap semiconductor like $\text{CH}_3\text{NH}_3\text{PbI}_3$ absorption coefficient can reach high values. This is shown from figure 16 drawn from values in Appendix IV.

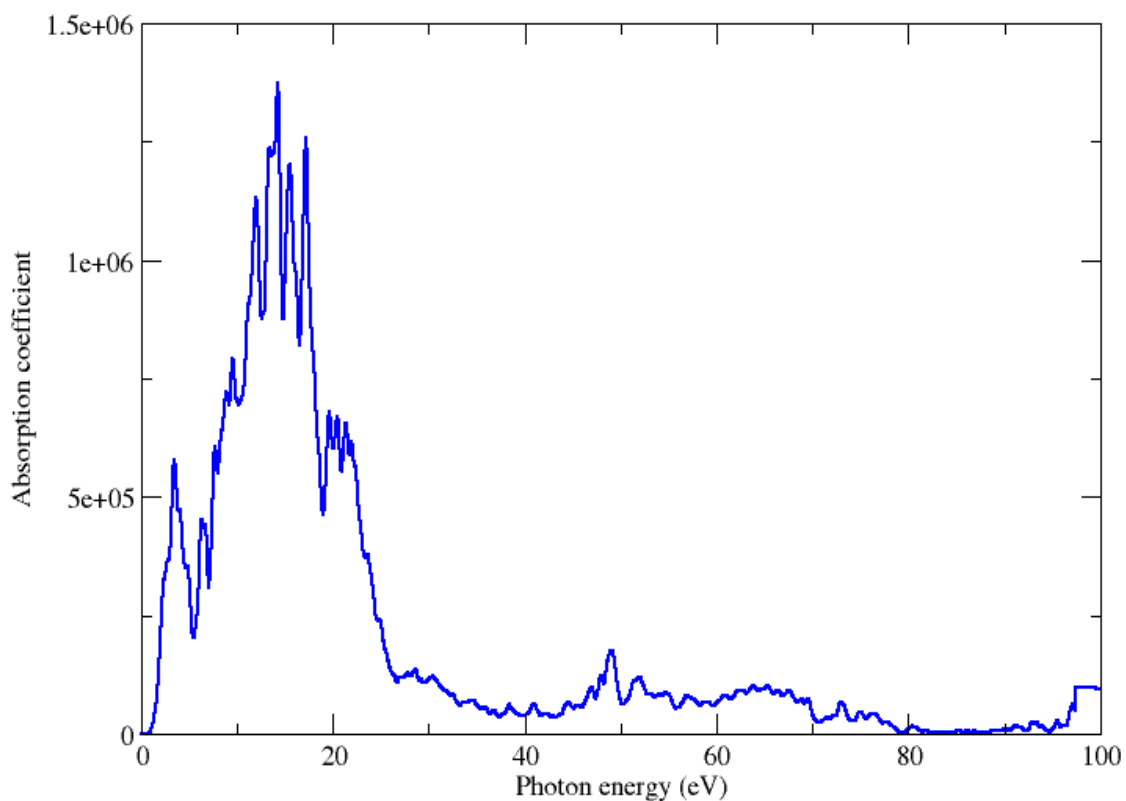


Figure 16: Absorption coefficient against Photon Energy

The high photovoltaic performance of $\text{CH}_3\text{NH}_3\text{PbI}_3$ is associated to optically high absorption characteristics. It is clear from Figure 16 that the material has high absorption ability. Its absorption coefficient is about $1.4 \times 10^6 \text{ cm}^{-1}$ for energy between 0 to 100 eV which contributes to effective utilization of solar radiation. This means that with high absorption coefficient, $\text{CH}_3\text{NH}_3\text{PbI}_3$ readily absorbs photons, which excite electrons from the valence band into the conduction band. In the solar spectrum the visible light is found within the range of wavelength $\lambda \approx 380\text{--}780 \text{ nm}$ which translates to energy of approximately 1.6-3.5 eV. The absorption coefficient within this region is $5.76 \times 10^5 \text{ cm}^{-1}$ as discusses in section 4.3 figure 18. The imaginary part of figure 17 indicates a maximum absorption of photon energy between 0- 5.0 eV, which is within the region where solar energy is utilized in a solar cell. $\text{CH}_3\text{NH}_3\text{PbI}_3$ has a band gap of 1.58eV, this means that only photons of energy equal to 1.58eV will be absorbed by the material. Photons of higher or lower energy value than the band gap is wasted.

The Real and Imaginary part of $\text{CH}_3\text{NH}_3\text{PbI}_3$

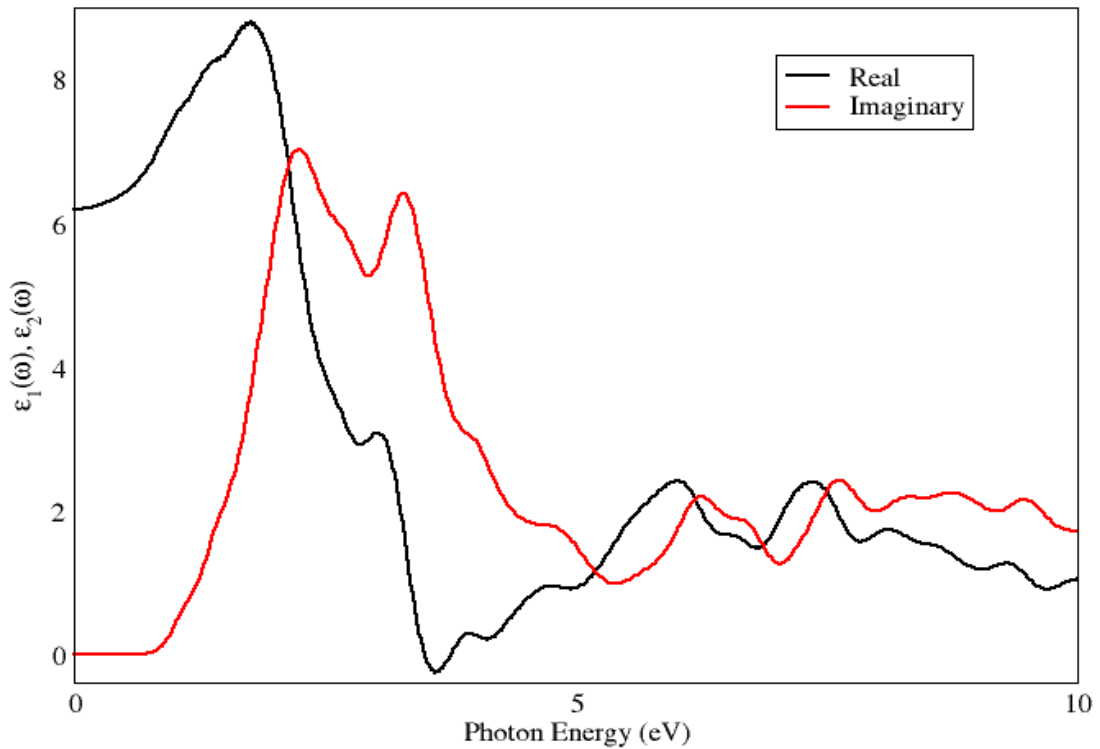


Figure 17: Real $\epsilon_1(\omega)$ and Imaginary $\epsilon_2(\omega)$ part against the Photon Energy

Figure 17 shows that appearance of a sharp peak of the imaginary part of the dielectric constant of the $\text{CH}_3\text{NH}_3\text{PbI}_3$ on implies the occurrence of strong absorption in this spectral region. The real part is related to the refractive index while the imaginary to absorption coefficient. A material with high dielectric constant has relatively less charge carrier recombination rate. As a result the overall performance of optoelectronic devices is enhanced.

4.3 Properties of $\text{CH}_3\text{NH}_3\text{PbI}_3$ for Photovoltaic Application

As discussed in Chapter 2 a good solar cell material should have a narrow and direct band gap. The results obtained from Figure 13 confirms that the material as a direct band gap at \mathbf{X} and small band gap of 1.58eV which can be tuned during fabrication through doping with other materials making it smaller and more suitable to be used as a solar cell material.

The lattice parameter was determined by optimization and found to be 6.39(Å). The value was found to be in good agreement with other theoretical and experimental work done on this material. Lattice parameter affects the band structure increasing or decreasing it will affect the value of the band gap energy. Therefore the correct value of lattice parameter is important in attaining a suitable band gap for use as photovoltaic material.

The ratio $\frac{B}{G}$, was estimated from average Voigt-Reuss-Hill approximation to be 2.08. The ratio is more than 1.75 showing that $\text{CH}_3\text{NH}_3\text{PbI}_3$ is a ductile material. Poisson's ratio calculated was found to be 0.25 which when rounded off to one decimal place is approximately equal to 0.3. The ratio $\frac{B}{G}$ and the Poisson's ratio are used to determine the brittleness and the ductility of a material. The result from the elastic constants confirms that $\text{CH}_3\text{NH}_3\text{PbI}_3$ is a ductile material. This means that the material can be molded during fabrication to different shapes and size therefore suitable to be used as a solar cell material.

In the solar spectrum the visible light is found within the range of wavelength $\lambda \approx 380 - 780$ nm and energy is $\sim 1.6-3.5$ eV. Visible light of the solar spectrum is what is absorbed and utilized by solar cell to produce electricity. Not all solar energy is absorbed but only photons with energy equal to the band gap. The absorption coefficient was found to be high ensuring maximum absorption of solar radiation. The output of absorption coefficient versus photon energy within the visible region is shown in figure 18.

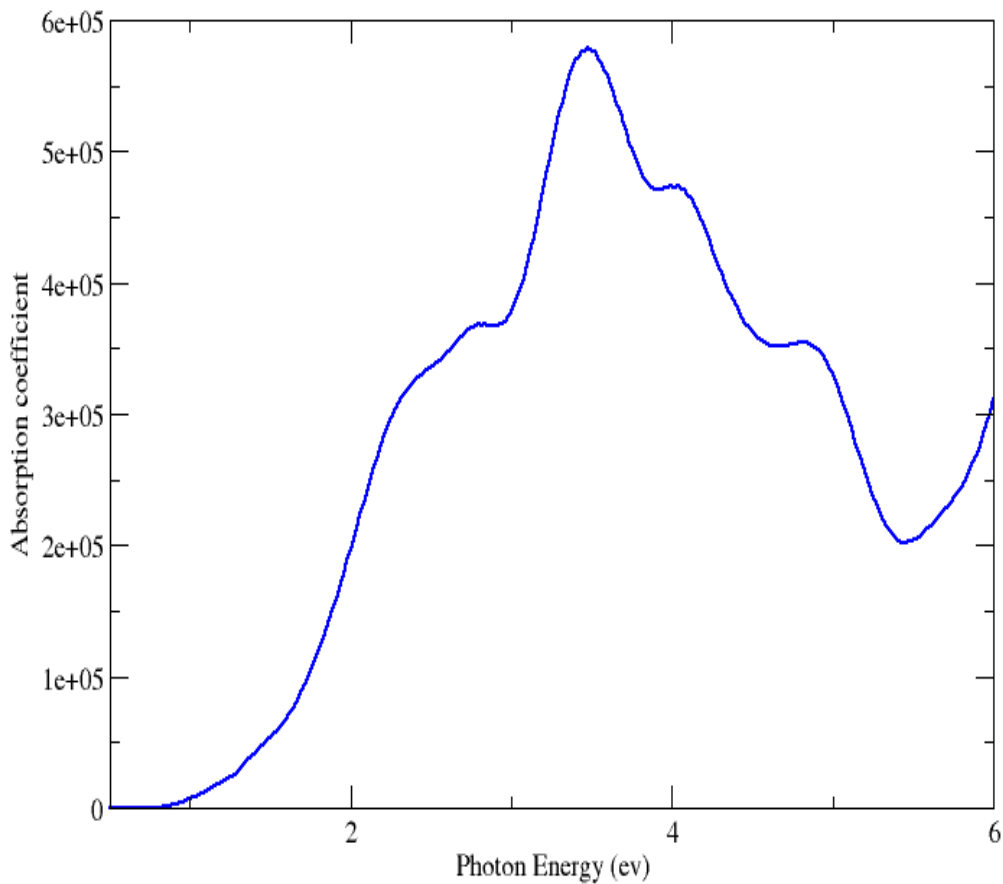


Figure 18: Absorption coefficient against photon energy (0 – 6eV)

Figure 18 indicates that at about 3.5 eV there is a peak in the absorption of the visible spectrum by $\text{CH}_3\text{NH}_3\text{PbI}_3$. The peak in figure 18 gives the absorption coefficient within the given range and it was found to be $5.76 \times 10^5 \text{ cm}^{-1}$ indicating maximum absorption. This value can be compared with the derived absorption coefficient done by Ball et al. (2015) of $1.0978 \times 10^5 \text{ cm}^{-1}$ and Phillips et al. (2015) of $8.1448 \times 10^4 \text{ cm}^{-1}$, which greatly depends on the range at which the energy or wavelength was measured from. The absorption coefficient determines how far into a material light of a particular wavelength or energy can pass through a material before it is absorbed. Absorption of solar energy will occur within the near UV region, visible region and near infra-red region between energy 0.886 eV–3.98 eV. This is equivalent to the wavelength of 1400nm – 380nm. This means that the material has a relatively wide absorption range as shown by the

wavelength. The high absorption coefficient of $\text{CH}_3\text{NH}_3\text{PbI}_3$ indicates that the material readily absorbs photons with energy equivalent to the band gap energy which excite electrons from valence band into the conduction band.

The band gap was found to be 1.58 eV, which is within the energy range of solar radiation to be absorbed. Photon energy from the sun with energy equal to 1.58eV will be absorbed and is sufficient to excite an electron from the conduction band to the valence band of $\text{CH}_3\text{NH}_3\text{PbI}_3$. The band gap and absorption coefficient of Silicon and $\text{CH}_3\text{NH}_3\text{PbI}_3$ are comparable and is given in Table 5.

Table 5: Comparison of the band gap and absorption coefficient of Silicon and $\text{CH}_3\text{NH}_3\text{PbI}_3$

Material	Band Gap	Absorption Coefficient
Silicon (Si)	1.14 eV Streetman et al.(2000)	$2.36 \times 10^6 \text{ cm}^{-1}$ (Range 1.0- 6 eV) Honsberg and Bowden, (2019)
Lead Iodide Perovskite ($\text{CH}_3\text{NH}_3\text{PbI}_3$)	1.58 eV	$5.76 \times 10^5 \text{ cm}^{-1}$ (Range 0 – 6eV)

The high absorption coefficient ($5.76 \times 10^5 \text{ cm}^{-1}$) of $\text{CH}_3\text{NH}_3\text{PbI}_3$ and its narrow band gap suggests that this material is good for application photovoltaic as intended in this research.

CHAPTER FIVE

SUMMARY, CONCLUSION AND RECOMMENDATION

5.1 Introduction

The objective of this thesis was to use first principle method in Density function theory to determine the electronic, mechanical and optical properties of $\text{CH}_3\text{NH}_3\text{PbI}_3$, and how these properties contribute in the photovoltaic application.

5.2 Summary

From the thesis, the following deductions are made;

In this section, the summary of the results of electronic, mechanical and optical properties of $\text{CH}_3\text{NH}_3\text{PbI}_3$ have been reported. The lattice parameter, band gap, elastic constants and optical constants (absorption and dielectric) were determined. Most of the results of these parameters are in agreement with both experimental and other theoretical computations so far done on this material.

Lattice parameter of $\text{CH}_3\text{NH}_3\text{PbI}_3$ was found to be 6.39 Angstroms. The band gap of $\text{CH}_3\text{NH}_3\text{PbI}_3$ was found to be a direct band gap of 1.58eV. From previous study, a good optical material should have a small tunable direct band gap which can be adjusted to give excellent power conversion efficiency.

The result from the elastic constants done compare well with previously done work and it confirms that $\text{CH}_3\text{NH}_3\text{PbI}_3$ is a ductile material. This means that it can be moulded to different shapes and size therefore suitable to be used as a solar cell material.

The optical constants which include absorption coefficient, real and imaginary components of the dielectric constant were calculated. There was however inadequate literature from experimental and DFT for the absorption coefficient to compare our

results to satisfaction. From this work it can be concluded that $\text{CH}_3\text{NH}_3\text{PbI}_3$ has high absorption coefficient which can make a good solar cell material.

The results obtained from this work are meaningful for designing solar cells of higher efficiency than silicon. The knowledge of absorption coefficients, lattice parameter, elastic constants and the band gap of materials helps engineers when choosing the suitable material for solar cell fabrication and design.

5.3 Conclusion

In conclusion, the findings from this work can give guidance for the future experimental work in the development of a potentially high performing solar cell absorber from $\text{CH}_3\text{NH}_3\text{PbI}_3$ material and also shed more light on fabricating perovskite PV cells with high efficiency and better performance.

5.4 Recommendation

This research work gives room to a number of unanswered questions for future study;

- i. A detailed analysis of other optical constants which include reflectance, conductance and transmittance among others to be done experimentally and by DFT so as to provide more information on the suitability of $\text{CH}_3\text{NH}_3\text{PbI}_3$ as a solar cell material.
- ii. This material $\text{CH}_3\text{NH}_3\text{PbI}_3$ is traditional, since ABX_3 can exist in other forms like; (A= Rb, Cs; B= Ge, Si, Sn, Pb; X=Br, Cl,I,) more analysis can be done on this materials to exploit their suitability as solar cell materials.
- iii. The study of electronic, mechanical and optical properties of tetragonal and orthorhombic phases of $\text{CH}_3\text{NH}_3\text{PbI}_3$ will shade more light on their suitability as a photovoltaic material.

REFERENCES

- Abdussamad Abbas, H. (2017). *Vapour Grown Perovskite Solar Cells*. (Doctoral Dissertation, Iowa State University).
- Abedin, M. I., Islam, A., & Hossain, Q. D. (2015, December). A self-adjusting Lin-Log Active pixel for wide dynamic range CMOS image sensor. In *2015 IEEE International Conference on Telecommunications and Photonics (ICTP)* (pp.1-4).
- Azarhoosh, P. (2017). The Optical and Electronic Properties of Organic-Inorganic Hybrid Perovskites. *Doctorate of Philosophy in Physics King's College London United Kingdom* 1-126.
- Ball, J. M., S. D., Stranks, M. T., Hörantner, S., Hüttner, W., Zhang, E. J. W., Crossland, I., Ramirez, M., Riede, M. B., Johnston, R. H., Friend, H., & Snaith, J. (2015). Optical Properties and limiting photocurrent of thin-film perovskite solar Cells, *Energy Environ. Sci* 8,602-609.
- Beltracchi, P. (2015). First-principles study of hybrid organic-inorganic perovskites for Photovoltaic applications, *A (Doctoral dissertation, Colorado School of Mines. Arthur Lakes Library)* 1-58.
- Berger, R. (2017). *Re: What's the Relationship between the Bond Length and the Cell Parameters for NiAs Structure?*<https://www.researchgate.net/post/Whats-the-relationship-between-the-bond-length-and-the-cell-parameters-for-NiAs-Structure/596fccfc5b495264b3399b15/citation/download>.
- Bretschneider, S. A., Weickert, J., Dorman, J. A., & Schmidt-Mende, L. (2014). Research Update: Physical and Electrical Characteristics of Lead Halide Perovskites for Solar Cell Applications. *APL Mater.* 2(4) 040701.
- Bharwal, A. (2018). *Hierarchical porous TiO2 and ionic liquid-like polysiloxane Electrolyte for solid state-Dye-Sensitized Solar Cells* (Doctoral dissertation, University Grenoble Alpes).
- Brivio, F., Butler, K. T., Walsh, A., & Van Schilfgaarde, M. (2014). Relativistic Quasi particle self-consistent electronic structure of hybrid halide perovskite Photovoltaic absorbers. *Physical Review B*, 89(15), 155204.
- Brivio, F., Walker, A. B., & Walsh, A. (2013). *APL Mater* 1, 042111. <http://dx.doi.org/10.1063/1.4824147>.
- Callister, W. D., & Rethwisch, D. G. (2007). Materials science and engineering: an Introduction. *Nature*, 7(2), 665-715.
- Capelle, K. (2006). A bird's-eye view of density-functional theory. *Brazilian Journal of Physics*, 36(4A), 1318-1343.
- Christiana, H., & Bowden, S. (2019) <https://www.pv-education.org/pvcdrom/pn-junctions/absorption-coefficient>.
- Ciucivara, A. I. (2007). *Density Functional Studies of Magnetic Semiconductors and Multiferroics* Doctoral dissertation.

- Dalven, R. (1973) *Empirical & Relation between Energy Gap and Lattice Constant in Cubic Semiconductors* University of California.
- Dang, Y., Liu, Y., Sun, Y., Yuan, D., Liu, X., Lu, W., & Tao, X. (2015). Bulk crystal Growth of hybrid perovskite material $\text{CH}_3\text{NH}_3\text{PbI}_3$. *CrystEngComm*, 17(3), 665-670.
- Deschler, F., Price, M., Pathak, S., Klintberg, L.E., Jarausch, D.D., Higler, R., Hüttner, S., Leijtens, T., Stranks, S.D., Snaith, H.J., Atatüre, M., Phillips, R.T., & Friend, R.H.J. (2014). *Phys. Chem. Lett*, 5, 1421.
- Dong, L., Sun, S., Deng, Z., Li, W., Wei, F., Qi, Y., Li, Y., Li, X., Lu, P., & Ramamurty, U. (2017). Elastic properties and thermal expansion of lead-free halide double Perovskite $\text{Cs}_2\text{AgBiBr}_6$. *Computational Materials Science*, 141, 46-58.
- Donev J.M.K.C. et al. (2015). Energy Education - Band gap [Online]. Available: https://energyeducation.ca/encyclopedia/Band_gap. 2020.
- Du, M. H. (2015). Density functional calculations of native defects in $\text{CH}_3\text{NH}_3\text{PbI}_3$: Effects of spin-orbit coupling and self-interaction error. *The Journal of Physical Chemistry Letters*, 6(8), 1461-1466.
- Even, J., Pedesseau, L., Jancu, J. M., & Katan, C. (2013). Importance of spin-orbit Coupling in hybrid organic/inorganic perovskites for photovoltaic applications. *The Journal of Physical Chemistry Letters*, 4(17), 2999-3005.
- Kerr, E. (2019). *The Future of Solar is Bright*. <http://sitn.hms.harvard.edu/flash/2019/future-solar-bright/>.
- Ezealigo, B. N., Nwanya, A. C., Ezugwu, S., Offiah, S., Obi, D., Osuji, R. U., & Ezema, F. I. (2017). Method to control the optical properties: Band gap energy of mixed halide Organo-lead perovskites. *Arabian Journal of Chemistry*.
- Faghihnasiri, M., Izadifard, M., & Ghazi, M.E. (2017). DFT study of mechanical Properties and stability of cubic methyl-ammonium lead halide perovskites ($\text{CH}_3\text{NH}_3\text{PBX}_3$, X = I, Br, Cl). *Journal of Physical Chemistry*.
- Feng, J. (2014). Mechanical properties of hybrid organic-inorganic $\text{CH}_3\text{NH}_3\text{BX}_3$ (B = Sn, Pb; X = Br, I) perovskites used in solar cell absorbers. *APL Materials*, 2(8), 081801.
- Fu, H., Li, D., Peng, F., Gao, T., & Cheng, X. (2008). Ab initio calculations of elastic Constants and thermodynamic properties of NiAl under high Pressures. *Computational Materials Science*, 44(2), 774-778.
- Gajdoš, M., Hummer, K., Kresse, G., Furthmüller, J., & Bechstedt, F. (2006). Linear Optical properties in the projector-augmented wave methodology. *Physical Review B*, 73(4), 045112.
- Giannozzi, P. S., Baroni, N., Bonini, M., Calandra, R., Car, C., Cavazzoni, D., Ceresoli, G.L., Chiarotti, M., Cococcioni, I., Dabo, A., Dal Corso, S., Fabris, G., Fratesi, S., de Gironcoli, R., Gebauer, U., Gerstmann, C., Gougoussis, A., Kokalj, M., & Lazzeri. (2009). Quantum ESPRESSO: a modular and open-source software project for quantum simulations of materials. *Journal of Physics: Condensed Matter* 21, 395502.

- Grancini, G., Marras, S., Prato, M., Giannini, C., Quarti, C., De Angelis, F., De Bastiani, M., Eperon, G.E., Snaith, H.J., Manna, L., & Petrozza, A. (2014). The impact of the crystallization processes on the structural and optical properties of hybrid Perovskite films for photovoltaics. *J. Phys. Chem. Lett.*, 5, 3836–3842.
- Green, M. A., How-Baillie, A., & Snaith, H. J. (2014). The emergence of perovskite solar cells. *Nature Photonics*, 8(7), 506.
- Gueymard, C. A. (2004). The sun's total and spectral irradiance for solar energy Applications and solar radiation models. *Solar Energy*, 76(4), 423-453.
- Ha, S.T., Liu, X., Zhang, Q., Giovanni, D., Sum, T.C., & Xiong, Q. (2014). Synthesis of Organic inorganic lead halide perovskite nano platelets: Towards high – Performance perovskite solar cells and optoelectronic devices. *Advanced Optical Materials*, 2(9), 838-844.
- Harrison, N.M (2001). *An Introduction to Density Function Theory*. [Http://www.ch.ic.ac.uk/Harrison/Teaching/DFT/NATO.pdf](http://www.ch.ic.ac.uk/Harrison/Teaching/DFT/NATO.pdf).
- Hebig, J.C., Kuhn, I., Flohre, J., & Kirchartz, T. (2016). Optoelectronic properties of $(\text{CH}_3\text{NH}_3)_3\text{Sb}_2\text{I}_9$ thin films for photovoltaic applications. *ACS Energy Letter*, 1(1), 309-314.
- Horváth, O., & Mikó, I.S. (1998). Equilibrium and photo redox chemistry of Tri- and Tetraiodoplumbate (II) complexes in acetonitrile. *Journal of Photochem. Photobiol*, 114, 95–101.
- Hohenberg, P., & Kohn, W. (1964). Inhomogeneous electron gas. *Physical Review*, 136(3B), B864.
- Honsberg, C.B., & Bowden, S.G. (2019). *Absorption Coefficient*. www.pveducation.org.
- Hu, M., Ge, C., Yu, J., & Feng, J. (2017). Mechanical and optical properties of Cs_4BX_4 (B=Pb, Sn; X=Cl, Br I) zero dimension perovskites. *Journal of Physical Chemistry* 7b10629? Src=recsys.
- Hybertsen, M. S., & Louie, S. G. (1987). Ab initio static dielectric matrices from the Density-functional approach. I. Formulation and application to Semiconductors and insulators. *Physical Review B*, 35(11), 5585.
- Isabella, O., Smets, A. H., & Zeman, M. (2014). Solar Energy-Fundamentals, Technology, and Systems. *Published by UIT Cambridge Ltd*, 83-98.
- Jellicoe, T.C., Richter, J.M., Glass, H.F.J., Tabachnyk, M., Brady, R., & Dutton, S. E. (2016). Synthesis and optical properties of lead-free cesium tin halide Perovskite nanocrystals. *Journal of the American Chemical Society*, 138, 2941-2944.
- Kanhere, P., Chakraborty, S., Rupp, C. J., Ahuja, R., & Chen, Z. (2015). Substitution Induced band structure shape tuning in hybrid perovskites $(\text{CH}_3\text{NH}_3)_{1-x}\text{Sn}_x\text{I}_3$ or efficient solar cell applications. *RSC Advances*, 5(130), 107497-107502.
- Kohn, W., & Sham, L. J. (1965). Self-consistent equations including exchange and Correlation effects. *Physical Review*, 140(4A), A1133.

- Kleinman, L., & Bylander, D. M. (1982). Efficacious form for model Pseudo potentials. *Physical Review Letters*, 48(20), 1425.
- Lee, M.M., Teuscher, J., Miyasaka, T., Murakami, T.N., & Snaith, H.J. (2012). Efficient Hybrid solar cells based on meso-superstructured organometal halide Perovskites. *Science*, 338, 643.
- Feng, J. (2014). Mechanical properties of hybrid organic-inorganic CH₃NH₃BX₃ (B= Sn, Pb; X= Br, I) perovskites for solar cell absorbers. *Apl Materials*, 2(8), 081801.
- Kothari, C.R (2004). *Research Methodology: Methods and Techniques*, (2nd Ed.). New Age International Publishers Ltd.
- Nelson, J. A. (2003). *The Physics of Solar Cells*. World Scientific Publishing Company.
- Phillips L.J. A. M., Rashed, R. E., Treharne, J., Kay, P., Yates, I., Mitrovic, A., Weerakkody, S., Hall, K., & Durose. K. (2015). Dispersion relation data for Methyl-Ammonium Lead triiodide perovskite deposited on a (100) silicon wafer Using A two-step Vapour-phase reaction process, *Data in Brief* 5, 926-928.
- Donev, J., Kailyn, S., & Jordan, H. (2015). *Energy Education - Band Gap*. https://energyeducation.ca/encyclopedia/Band_gap.
- Leisure, R. G. (2004). *Hydrogen–Metal Systems: Elastic Properties* 1-5.
- Lin, Q., Armin, A., Burn, P.L., & Meredith, P. (2016). Organo-halide perovskites for solarenergy conversion. *Accounts of Chemical Research*, 49, 545–553.
- Leon, V. D.(2008). *Quantum Mechanics for Engineers, FAMU-FSU College of Engineering, 9.3 the Hartree-Fock Approximation*.
- Manser, J.S., Reid, B., & Kamat, P.V. (2015). Evolution of organic–inorganic lead halideperovskite from solid-state Iodoplumbate complexes. *Journal of Phys. Chem. C*, 119, 17065–17073.
- Manser, J.S., Saidaminov, M.I., Christians, J.A., Bakr, O.M., & Kamat, P.V. (2016). Lead halide perovskites for solar energy conversion. *Accounts of Chemical Research*, 49, 330-338.
- Manyali, G. S. (2014). A computational study of layered and superhard carbon-nitrogen Material. *Doctoral dissertation, Faculty of Science, University of the Witwatersrand, Johannesburg*, 1-80.
- Manyali, G. S., Warmbier, R., Quandt, A., & Lowther, J. E. (2013). Ab initio study of Elastic properties of super hard and graphitic structures of C₃N₄. *Computational Materials Science*, 69, 299-303.
- Marshall, K.P., Walton, R.I., & Hatton, R.A.J. (2015). Tin perovskite / fullerene planar Layer photovoltaics: improving the efficiency and stability of lead-free devices *Journal of Material Chemistry*, 3, 11631.

- Mayengbam, R., Tripathy, S. K., & Palai, G. (2018). First-Principle Insights of Electronic and Optical Properties of Cubic Organic–Inorganic $\text{MAGe}_x\text{Pb}_{(1-x)}$ Perovskites for Photovoltaic Applications. *The Journal of Physical Chemistry C*, *122*(49), 28245-28255.
- Meng, X. Y., Liu, D. Y., & Qin, G. W. (2018). Band engineering of multicomponent Semiconductors: a general theoretical model on the anion group. *Energy & Environmental Science*, *11*(3), 692-701.
- Miyata, K., Meggiolaro, D., Trinh, M.T., Joshi, P.P., Mosconi, E., Jones, S.C., Angelis, F., & Zhu, X.Y. (2017). Large polarons in lead halide perovskites. *Science Advances*, *3*(8). [Org/content/3/8e1701217](https://doi.org/10.1126/sciadv.1701217).
- Monkhorst, H. J., & Pack, J. D. (1976). Special points for Brillouin-zone Integrations. *Physical Review B*, *13*(12), 5188.
- Mouhat, F., & Coudert, F. X. (2014). Necessary and sufficient elastic stability conditions in various crystal systems. *Physical review B*, *90*(22), 224104.
- Murnaghan, F. D. (1944). The compressibility of media under extreme pressures. *Pro-Academy of Sciences*, *30*(9), 244-247.
- Navaretti, P. (2018). Re: *What is the Wavelength which is corresponding to Band Gap Energy?* <https://www.researchgate.net/post/What-is-the-wavelength-which-is-corresponding-to-band-gap-energy/5aeaca3b10569f1c98214ab8/citation/download>.
- Noel, N.K., Stranks, S.D., Abate, A., Wehrenfennig, C., Guarneri, S., Haghighirad, A.A., Sadhanala, A., Eperon, G.E., Pathak, S.K., Johnston, M.B., Petrozza, A., Herz, L.M., & Snaith, H.J. (2014). Lead-free organic-inorganic tin halide perovskites for photovoltaic applications. *Energy Environ. Sci.*, *7*, 3061-3068.
- Noh, J.H., Im, S.H., Heo, J.H., Mandal, T.N., & Seok, S. (2013). Chemical management for Colourful, efficient, and stable inorganic-organic hybrid nanostructured solar Cells. *Nano Lett.*, *13*, 1764–1769.
- Ondzibou, N. G. (2014). Computational study of structural, electronic and optical Properties of Molybdenum Chalcogenides. *Masters Dissertation, University of Witwaters Rand*.
- Pazoki, M., Rockert, A., Wolf, M.J., Imani, R., Edvinsson, T., & Kullgren, J. (2017). Electronic structure of organic-inorganic lanthanide iodide perovskite solar cell materials. *Journal of Materials Chemistry*, *44*, 22837-23384.
- Perdew, J. P., Burke, K., & Ernzerhof, M. (1996). Generalized gradient Approximation made simple. *Physical Review Letters*, *77*(18), 3865.
- Phillips L.J., A. M. Rashed, R. E. Treharne, J. Kay, P., Yates, I., Mitrovic, A., Weerakkody, S., Hall, K., & Durose. (2015). Dispersion relation data for Methyl-Ammonium Lead triiodide perovskite deposited on a (100) silicon wafer Using a two-step Vapour-phase reaction process, *Data in Brief*, *5*, 926-928.
- Phillippe, B., Park, B., Lindblad, R., & Rensmo, H. (2015). Chemical and electronic structure characterization of lead halide perovskites and stability behaviour

- Under different exposures—a photoelectron spectroscopy investigation .*Chem. Mater.* 27 (5), 1720–1731.
- Prasanna, R., Gold-Parker, A., Leijtens, T., Conings, B., Babayigit, A., Boyen, H. G., & McGehee, M. D. (2017). Band gap tuning via lattice contraction and octahedral Tilting in perovskite materials for photovoltaics. *Journal of the American Chemical Society*, 139(32), 11117-11124.
- Pugh, S. F. (1954). XCII. Relations between the elastic moduli and the plastic properties of polycrystalline pure metals. *The London, Edinburgh, and Dublin Philosophical Magazine and Journal of Science*, 45(367), 823-843.
- Qarony, W., Jui, Y.A., Das, G., Mohsin, T., Hossain, M.I., & Islam, S.N. (2015). Optical analysis in $\text{CH}_3\text{NH}_3\text{PbI}_3$ and $\text{CH}_3\text{NH}_3\text{PbI}_2\text{Cl}$ based thin-film perovskite solar Cell. *American Journal of Energy Research*, 3(2), 19-2
- Ravindran, P., Fast, L., Korzhavyi, P. A., Johansson, B., Wills, J., & Eriksson, O. (1998). Density functional theory for calculation of elastic properties of orthorhombic crystals. *Journal of Applied Physics*, 84(9), 4891-4904.
- Sadhanala, A., Deschler, F., Thomas, T.H., Dutton, S.E., Goedel, K.C., Hanusch, Lai, M.L., Steiner, U., Bein, T., Docampo, P., Cahen, D., & Friend, R.H.(2014).*J. Phys. Chem. Lett.*, 5, 2501.
- Sakurai, J. J., & Napolitano, J. (2014). *Modern Quantum Mechanics* 185. Pearson. Saliba, M., Matsui, T., Seo, J.Y., Domanski, K., Correa-Baena, J.P., Nazeeruddin, M.K.,
- Zakeeruddin, S.M., Tress, W., Abate, A., Hagfeldt, A., & Grätzel, M. (2016). Cesium-Containing Triple Cation Perovskite Solar Cells: Improved stability, Reproducibility and high efficiency. *Energy Environ. Sci.*, 9, 1989-1997.
- Sham, L. J., & Rice, T. M. (1966). Many-particle derivation of the effective-mass Equation for the Wannier exciton. *Physical Review*, 144(2), 708.
- Sifuna, S.J. (2017) Dental filling materials in the negative and near zero thermal Expansion regimes: Ab initio study on Scandium Trifluoride .*A Masters Study in Masinde Muliro University of Science and Technology, Kakamega*, 1-64.
- Sifuna, J., García-Fernández, P., Manyali, G. S., Amolo, G., & Junquera, J. (2020). First-Principles study of two-dimensional electron and hole gases at the head-to-head and tail-to-tail 180° domain walls in PbTiO_3 ferroelectric thin films. *Physical Review B*, 101(17), 174114.
- Soler, J. M., Artacho, E., Gale, J. D., García, A., Junquera, J., Ordejón, P., & Sánchez-Portal. (2002). The SIESTA method for ab initio order-N materials Simulation. *Journal of Physics: Condensed Matter*, 14(11), 2745.
- Stamplecoskie, K.G., Manser, J.S., & Kamat, P.V. (2015). Dual nature of the excited State in organic–inorganic lead halide perovskites. *Energy Environ. Sci.*, 8, 208–215.
- Stampfl, C., & Van de Walle, C. G. (1999). Density-functional calculations for III-V nitrides using the local-density approximation and the generalized Gradient approximation. *Physical Review B*, 59(8), 5521.

- Streetman, Ben G.; Sanjay Banerjee (2000). *Solid State Electronic Devices* (5th Ed.). Prentice Hall. p. 524. ISBN 0-13-025538-6.
- Sun, S., Isikgor, F.H., Deng, Z., Wei, F., Kieslich, G., Bristowe, P.D., Ouyang, J., & Cheetham, A.K. (2017). Factors influencing the mechanical properties of formamidinium lead halides and related hybrid perovskites. *Chem*, 10(19), 3740-3745.
- Tang, H., He, S., & Peng, C. (2017). A Short Progress Report on High-Efficiency Perovskite Solar Cells. *Nanoscale Research Letters*, 12(1), 410. <https://doi.org/10.1186/s11671-017-2187-5>.
- Tanner D.B. (2016). Optical Effects in Solids, Department of Physics, University of Florida.
- Takaba, H., Kimura, S., & Alam, K. (2017). Crystal and electronic structures of substituted halide perovskites based on density functional calculation and molecular dynamics. *Journal of Chemical Physics*, 146, 22-28.
- Tao, S.X., Cao, X., & Bobbert, P.A. (2017). Accurate and efficient band gap predictions of metal halide perovskites using the DFT-1/2 method: GW accuracy with DFT expense. *Scientific Reports*, 7, 14386.
- Troullier, N., & Martins, J. L. (1991). Efficient pseudo potentials for plane-wave Calculations. *Physical Review B*, 43(3), 1993.
- Verhoeven, G. (2017). The reflection of two fields: electromagnetic radiation and its role in (aerial) imaging. *AARGNEWS*, 55, 13-18.
- Wang, L., Wang, K., & Zou, B. (2016). Pressure-induced structural and optical properties of organometal halide perovskite-based formamidinium lead bromide. *Journal of Physical Chemistry Letter*, 7(13), 255-2562.
- Wang, Y., Gould, T., Dobson, J. F., Zhang, H., Yang, H., Yao, X., & Zhao, H. (2013). Density functional theory analysis of structural and electronic properties of orthorhombic perovskite CH₃NH₃PbI₃. *Physical Chemistry Chemical Physics*, 16(4), 1424-1429.
- Weik M.H. (2000). *Absorption Index*. In: *Computer Science and Communications Dictionary* Springer, Boston, MA.
- Williams, S.T., Zuo, F., Chueh, C.C., Liao, C.Y., Liang, P.W., & Jen, A.K.Y. (2014). Role of Chloride in the morphological evolution of organo-lead halide perovskite thin films. *American Chemical Society Nano*, 8, 10640–10654.
- Zekry, A. (2017). https://www.researchgate.net/post/How_does_band_gap_of_a_Semiconductor_change_with_the_lattice_constant_Please_explain_the_physical_significance/59d373c6eeae393a401b512c/citation/download.
- Zeng, Z., Hansen, M. H., Greeley, J. P., Rossmeisl, J., & Björketun, M. E. (2014). Ab initio Thermodynamic Modelling of Electrified Metal–Oxide Interfaces: Consistent Treatment of Electronic and Ionic Chemical Potentials. *The Journal of Physical Chemistry C*, 118(39), 22663-22671.

- Zhang, Q., Hao, F., Li, J., Zhou, Y., Wei, Y., & Lin, H. (2018). Perovskite solar cells: Must lead be replaced—and can it be done? *Science and Technology of Advanced Materials* 19(1), 425-442.
- Zhang, Y.Y., Chen, S., Xu, P., Xiang, H., Gong, X.G., Walsh, A., & Wei, S.H. (2015). *Intrinsic Instability of the Hybrid Halide Perovskite Semiconductor CH₃NH₃PbI₃*.
- Zhu, H. X., & Liu, J. M. (2016). Electronic structure of organometal halide perovskite CH₃NH₃ Bi I₃ and optical absorption extending to infrared region *Scientific Reports*, 6, 37425.<http://sitn.hms.harvard.edu/flash/2019/>

APPENDICES

Appendix I: Input file for pwscf code: Ecut.in,k-points.in and alat.in

& CONTROL

```
title = 'cubic_CH3NH3PbI3',  
calculation = 'scf',  
restart_mode = 'from_scratch',  
    pseudo_dir = './',  
outdir = './tmp',  
    prefix = 'pseudo',  
    tstress = .true.,  
tpnfor = .true.,
```

/

&SYSTEM

```
ibrav = 0,  
    celldm(1) = 12.0772387957,  
nat = 12 ,  
ntyp = 5 ,  
nbnd = 50 ,  
ecutwfc = 40.0 ,  
ecutrho = 500.0 ,  
occupations = 'smearing',  
smearing = 'marzari-vanderbilt',  
degauss = 0.0075 ,  
    !london_s6 = 0.750 ,  
    ! london_rcut = 50.0 ,  
    ! noncolin = .true. ,  
    ! lda_plus_u = .false. ,  
    ! lspinorb = .true. ,  
    ! nosym = .true. ,
```

/

& ELECTRONS

```
conv_thr = 1.0D-7 ,
```

/

ATOMIC_SPECIES

Pb 207.200 Pb.pbe-mt_fhi.UPF

I 126.900 I.pbe-mt_fhi.UPF

H 1.008 H.pbe-mt_fhi.UPF

C 12.011 C.pbe-mt_fhi.UPF

N 14.007 N.pbe-mt_fhi.UPF

ATOMIC_POSITIONS {crystal}

C 0.3939882648252961 0.4998165502286085 0.4578307086810938

N 0.6090744378334350 0.5000072812331666 0.5477685929486071

H 0.4101503344735065 0.4996421926480608 0.2857772518934283

H 0.3086756133568471 0.6447043733807547 0.5110306384926346

H 0.3088856672784672 0.3549521469503247 0.5113014134206253

H 0.6962691547534092 0.6357485658144455 0.5015129819664779

H 0.6964106005070789 0.3642097749426654 0.5017817996551273

H 0.6063401459460280 0.5001870434389417 0.7112184893396645

Pb 0.9448835519577230 0.9999795897298682 0.9776228940296079

I 0.9094873486598019 0.9999820990246278 0.4751454839169895

I 0.8992708791277906 0.4999580210910821 0.0236644354684188

I 0.4323428768805755 0.9999948727175436 0.9224794036872126

K_POINTS {automatic}

13 13 13 0 0 0

Appendix II: Input file for pwscf code: Pseudo-Cubic structure

```
&CONTROL
title = 'cubic_CH3NH3PbI3' ,
calculation = 'scf' ,
    restart_mode = 'from_scratch' ,
    pseudo_dir = './' ,
outdir = './tmp' ,
prefix = 'pseudo' ,
tstress = .true. ,
tprnfor = .true. ,
/
```

&SYSTEM

```
ibrav = 0 ,
celldm(1) = 12.0772387957 ,
nat = 12 ,
ntyp = 5 ,
nbnd = 50 ,
ecutwfc = 50.0 ,
ecutrho = 500.0 ,
occupations = 'smearing' ,
smearing = 'marzari-vanderbilt' ,
degauss = 0.0075 ,
    !london_s6 = 0.750 ,
    ! london_rcut = 50.0 ,
    ! noncolin = .true. ,
    ! lda_plus_u = .false. ,
    ! lspinorb = .true. ,
    ! nosym = .true. ,
```

&ELECTRONS

```
conv_thr = 1.0D-7 ,/
```

ATOMIC_SPECIES

```
Pb 207.200 Pb.pbe-mt_fhi.UPF
```

```

I 126.900 I.pbe-mt_fhi.UPF
H 1.008 H.pbe-mt_fhi.UPF
C 12.011 C.pbe-mt_fhi.UPF
N 14.007 N.pbe-mt_fhi.UPF
ATOMIC_POSITIONS {crystal}
C 0.3939882648252961 0.4998165502286085 0.4578307086810938
N 0.6090744378334350 0.5000072812331666 0.5477685929486071
H 0.4101503344735065 0.4996421926480608 0.2857772518934283
H 0.3086756133568471 0.6447043733807547 0.5110306384926346
H 0.3088856672784672 0.3549521469503247 0.5113014134206253
H 0.6962691547534092 0.6357485658144455 0.5015129819664779
H 0.6964106005070789 0.3642097749426654 0.5017817996551273
H 0.6063401459460280 0.5001870434389417 0.7112184893396645
Pb 0.9448835519577230 0.9999795897298682 0.9776228940296079
I 0.9094873486598019 0.9999820990246278 0.4751454839169895
I 0.8992708791277906 0.4999580210910821 0.0236644354684188
I 0.4323428768805755 0.9999948727175436 0.9224794036872126

K_POINTS {automatic}
13 13 13 0 0 0
CELL_PARAMETERS {alat}
1.0 0.0 0.0
0.0 1.0 0.0

```

Appendix III: Results of Lattice parameter, energy, pressure and enthalpy

equation of state: murnaghan. chisq = 0.5599D-12
 # V0 = 1719.65 a.u. ^3, k0= 384 kbar, dk0= 3.75 d2k0= 0.000 emin = -257.94108
 # V0 = 254.83 Ang^3, k0= 38.4GPa

```
#####
###
# Vol.      E_calc   E_fit   E_diff  Pressure  Enthalpy
# a.u. ^3   Ry       Ry      Ry      GPa       Ry
#####
###
```

# Vol. a.u. ^3	E_calc Ry	E_fit Ry	E_diff Ry	Pressure GPa	Enthalpy Ry
1593.72	-257.92748	-257.92747	-0.00000	3.38	-257.56105
1614.26	-257.93175	-257.93175	0.00000	2.74	-257.63075
1634.98	-257.93518	-257.93518	-0.00000	2.14	-257.69776
1655.88	-257.93780	-257.93780	-0.00000	1.56	-257.76218
1676.95	-257.93964	-257.93964	-0.00000	1.01	-257.82413
1698.20	-257.94072	-257.94072	-0.00000	0.49	-257.88372
1719.63	-257.94108	-257.94108	0.00000	0.00	-257.94104
1741.24	-257.94073	-257.94073	0.00000	-0.47	-257.99619
1763.03	-257.93971	-257.93971	-0.00000	-0.91	-258.04925

Appendix IV: Absorption coefficient. Out

0.0000000000000000	0.0000000000000000
1.9999978624805612E-002	0.24988928890946985
3.9999957249611223E-002	0.56433762654535935
5.9999935874416835E-002	0.93880409035995438
7.9999914499222446E-002	1.3637363347978548
9.9999893124028058E-002	1.8249222411118071
0.11999987174883367	2.3043054549207893
0.13999985037363930	2.7814219599502179
0.15999982899844489	3.2350568559897952
0.17999980762325052	3.6451955731050467
0.19999978624805612	3.9947583852990274
0.21999976487286174	4.2711463915435965
0.23999974349766734	4.4672020674000823
0.25999972212247296	4.5816254372279861
0.27999970074727859	4.6187371776105204
0.29999967937208416	4.5876703585826943
0.31999965799688979	4.5011851286911568
0.33999963662169541	4.3742003031563428
0.35999961524650104	4.2224078018739917
0.37999959387130661	4.0610222072591107
0.39999957249611223	3.9040452136353627
0.41999955112091786	3.7640632567371792
0.43999952974572348	3.6529455519580702
0.45999950837052905	3.5836006104679035
0.47999948699533468	3.5733897799420808
0.49999946562014030	3.6499273957827034
0.51999944424494593	3.8606612348911162
0.53999942286975156	4.2882586975166621
0.55999940149455718	5.0747471444112238
0.57999938011936270	6.4585256370478810
0.59999935874416832	8.8291054474426058

0.61999933736897395	12.805996207568926
0.63999931599377957	19.346607905096381
0.65999929461858520	29.890970541086375
0.67999927324339082	46.538939588370894
0.69999925186819645	72.272255963276436
0.71999923049300207	111.17399161491070
0.73999920911780759	168.70657806092615
0.75999918774261321	251.82732574133144
0.77999916636741884	369.29721031168708
0.79999914499222446	531.28329214132305
0.81999912361703009	749.89184290299875
0.83999910224183572	1037.2955829484670
0.85999908086664134	1407.5441140056985
0.87999905949144697	1871.1235629043078

Appendix V: University Authorization Letter



INSTITUTE OF POST GRADUATE STUDIES

Private Bag - 20157
KABARAK, KENYA
E-mail: directorpostgraduate@kabarak.ac.ke

Tel: 0203511275
Fax: 254-51-343012
www.kabarak.ac.ke

12th February, 2018

TO WHOM IT MAY CONCERN

Dear Sir/Madam,

RE: TRUPHENA J. KIPKWARWAR - REG NO. GMS/M/0936/08/16

The above named is a Master student at Kabarak University in the School of Computer Science and Bioinformatics, specializing in Master of Science in Physics. She has successfully defended her thesis proposal and is currently preparing to do field research.

Any assistance accorded to her will be highly appreciated.

Thank you.

Yours faithfully,

Dr. Esther J. Kibor
ACTING DIRECTOR - (POST-GRADUATE STUDIES)



Kabarak University Moral Code

As members of Kabarak University family, we purpose at all times and in all places, to set apart in one's heart, Jesus as Lord. (1 Peter 3:15)



Kabarak University is ISO 9001:2015 Certified

Appendix IV: KUREC Clearance



KABARAK UNIVERSITY RESEARCH ETHICS COMMITTEE

Private Bag - 20157
KABARAK, KENYA
Email: kurec@kabarak.ac.ke

Tel: 254-51-343234/5
Fax: 254-051-343529
www.kabarak.ac.ke

OUR REF: KABU01/KUREC/001/01/04/21

6th May, 2021

Truphena K. Jepkorir,
Kabarak University,
Dear Truphena,

SUBJECT: ETHICS REVIEW DECISION

KUREC received application for a protocol titled "AB INITIO STUDY OF ELECTRONIC, OPTICAL AND MECHANICAL PROPERTIES OF LEAD HALIDE PEROVSKITES FOR OPTICAL PERFORMANCE OF SOLAR CELL" on 18th April, 2021; reviewed and discussed it during a meeting held on 3rd May, 2021 at 1000 Hours. The committee has considered the application in accordance with the Kabarak University procedures on review of research protocols for ethical clearance and decided as follows:

1. PROPOSED STUDY SITE

SIMULATION STUDY

2. KUREC DECISION

Approved for data collection for a period of ONE year from 6th May, 2021

This approval is subject to the following conditions:

- i. The researcher shall obtain a RESEARCH PERMIT from NACOSTI before commencement of data collection;
- ii. The researcher shall immediately notify KUREC in case of any adjustments to the protocol;
- iii. The researcher shall within 7 days of occurrence notify KUREC of any adverse events associated with the conduct of this study;
- iv. The researcher shall submit the study progress reports after every 6 months and a full report at completion of the study/project

Please confirm that you agree with the decision and conditions of the committee by signing and returning a copy of this letter to KUREC within 5 working days.

Thank you.

Sincerely,

Prof. Jackson Kitetu PhD.
KUREC-Chairman

Cc Vice Chancellor
DVC-Academic & Research
Registrar-Academic & Research
Director-Research Innovation & Outreach
Institute of Post Graduate Studies



I, TRUPHENA K. JEPKORIR.....confirm that I have read and understood the conditions due to this approval and that I shall abide by them whatsoever.

Signature

06/05/2021
Date

As members of Kabarak University family, we purpose at all times and in all places, to set apart in one's heart, Jesus as Lord.
(1 Peter 3:15)



Kabarak University is ISO 9001:2015 Certified

Appendix V: NACOSTI Research Permit

 <p>REPUBLIC OF KENYA NATIONAL COMMISSION FOR SCIENCE, TECHNOLOGY & INNOVATION</p>	 <p>NATIONAL COMMISSION FOR SCIENCE, TECHNOLOGY & INNOVATION</p>
Ref No: 405544	Date of Issue: 11/May/2021
RESEARCH LICENSE	
	
<p>This is to Certify that Ms. truphena JEPKORIR kiplkworkwar of Kabarak University, has been licensed to conduct research in Nakuru on the topic: AB INITIO STUDY OF ELECTRONIC, OPTICAL AND MECHANICAL PROPERTIES OF LEAD HALIDE PEROVSKITES FOR OPTICAL PERFORMANCE OF SOLAR CELL for the period ending :11/May/2022.</p>	
License No: NACOSTI/P/21/10559	
Applicant Identification Number	Director General NATIONAL COMMISSION FOR SCIENCE, TECHNOLOGY & INNOVATION
	Verification QR Code
	
<p>NOTE: This is a computer generated License. To verify the authenticity of this document, Scan the QR Code using QR scanner application.</p>	

THE SCIENCE, TECHNOLOGY AND INNOVATION ACT, 2013

The Grant of Research Licenses is Guided by the Science, Technology and Innovation (Research Licensing) Regulations, 2014

CONDITIONS

1. The License is valid for the proposed research, location and specified period
2. The License any rights thereunder are non-transferable
3. The Licensee shall inform the relevant County Director of Education, County Commissioner and County Governor before commencement of the research
4. Excavation, filming and collection of specimens are subject to further necessary clearance from relevant Government Agencies
5. The License does not give authority to transfer research materials
6. NACOSTI may monitor and evaluate the licensed research project
7. The Licensee shall submit one hard copy and upload a soft copy of their final report (thesis) within one year of completion of the research
8. NACOSTI reserves the right to modify the conditions of the License including cancellation without prior notice

National Commission for Science, Technology and Innovation
off Walyaki Way, Upper Kabete,
P. O. Box 30623, 00100 Nairobi, KENYA
Land line: 020 4007000, 020 2241349, 020 3310571, 020 8001077
Mobile: 0713 788 787 / 0735 404 245
E-mail: dg@nacosti.go.ke / registry@nacosti.go.ke
Website: www.nacosti.go.ke

Appendix VII: Publications, Workshops and Conferences

Publications

1. Kipkwarkwar J. Truphena, Nyawere W.O.Philip & Maghanga Christopher. (2019). *Ab initio* Study of Electronic Properties of Lead Halide Perovskite for Optical Performance of Solar Cell. Kabarak University Journal, 45-53.

Workshops and Conferences

- Participation in a One-day hands on Workshop on Density –Functional Theory and Applications held on 5th July 2019 at Kabarak University, Nakuru, Kenya.
- Kabarak University International Research Conference on Basic Sciences held from 17th -18th September 2019 at Kabarak University, Kenya.
- Attended and Participated in the Regional Africa School of Electronic Structure Methods and Application (RASESMA) Conference with ABINIT from 27th- 31st January 2020, held in The University of Rwanda, Kigali, Rwanda.
- Attended and Participated in a two-day intensive workshop on Density-Functional Theory and beyond a held at The Catholic University of Eastern Africa (CUEA) from 5th -6th March 2020.